Title: ARID1A Maintains Differentiation of Pancreatic Ductal Cells and Inhibits Development of Pancreatic Ductal Adenocarcinoma in Mice

Short title: *Arid1a* suppresses IPMN and PDAC formation

Authors: Yoshito Kimura[1], Akihisa Fukuda[1], Satoshi Ogawa[1], Takahisa Maruno[1], Yutaka Takada[1], Motoyuki Tsuda[1], Yukiko Hiramatsu[1], Osamu Araki[1], Munemasa Nagao[1], Takaaki Yoshikawa[1], Kozo Ikuta[1], Takuto Yoshioka[1], Zong Wang[2], Haruhiko Akiyama[3], Christopher V. Wright[4], Kyoichi Takaori[5], Shinji Uemoto[5], Tsutomu Chiba[1], Hiroshi Seno[1]

[1]Department of Gastroenterology and Hepatology, Kyoto University Graduate School of Medicine, 54 Shogoin-Kawahara-cho, Sakyo-ku, Kyoto 606-8507 Japan.

[2]Department of Cardiac Surgery, Cardiovascular Research Center, University of Michigan, 2800 Plymouth Road, An Arbor, MI 48109, USA.

[3]Department of Orthopaedics, Gifu University, 1-1 Yanagido, Gifu City 501-1194,

Japan.

[4]Program in Developmental Biology and Department of Cell and Developmental Biology, Vanderbilt University School of Medicine, Nashville, Tennessee 37240, USA.

[5]Division of Hepatobiliary-Pancreatic Surgery and Transplantation, Department of Surgery, Kyoto University Graduate School of Medicine, 54 Shogoin-Kawahara-cho, Sakyo-ku, Kyoto 606-8507 Japan.

Grant support: This work was supported in part by Grants-in-Aid KAKENHI (25112707, 26293173, 14J03460, 16K09394, 16K15427, and 17J05511); a research program as part of the Project for Development of Innovative Research on Cancer Therapeutics (P-Direct) from the Ministry of Education, Culture, Sports, Science, and Technology and the Japan Society for the Promotion of Science. It was also supported by the Naito Foundation (2013-007); Princess Takamatsu Cancer Research Fund (13-24514); the Mochida Foundation (2017bvAg); the Mitsubishi Foundation (281119); the Takeda Foundation (201749741). It was also supported by an NIH grant (R01HL109054) to Zhong

Wang.

Abbreviations: AT rich interactive domain 1A (ARID1A), Brahma related gene 1 (BRG1), pancreatic intraepithelial neoplasia (PanIN), intraductal papillary mucinous neoplasm (IPMN), pancreatic ductal adenocarcinoma (PDAC), pancreatic ductal cells (PDCs)

Correspondence: Akihisa Fukuda

Department of Gastroenterology and Hepatology, Kyoto University Graduate School of Medicine, 54 Shogoin-Kawahara-cho, Sakyo-ku, Kyoto 606-8507 Japan.

E-mail: fukuda26@kuhp.kyoto-u.ac.jp

Phone: +81-75-751-4319

Fax: +81-75-753-4303

Disclosures: The authors disclose no conflict of interest.

Transcript Profiling: GSE96926

Author contributions: Y.K. and A.F. conceived and designed the study. O.S., T.M., Y.T., M.T., K.I., T.Y., Y.H., O.A., M.N., and T.Y. performed the experiments

and analyzed the data. H.A. generated the *Sox9OE* mice. C.V.W. generated the *Ptf1a-Cre^{ER}* mice. Y.K., T.M., M.T., K.T., and S.U. contributed reagents/materials/analysis tools. Y.K. wrote the manuscript, and A.F., T.C., and H.S. revised it.

Abstract

Background & Aims: The AT-rich interaction domain 1A gene (*ARID1A*) encodes a protein that is part of the large ATP-dependent chromatin remodeling complex SWI/SNF and is frequently mutated in human pancreatic ductal adenocarcinomas (PDACs). We investigated the functions of ARID1A during formation of PDACs in mice.

Methods: We performed studies with *Ptf1a*-Cre; *Kras*^{G12D} mice, which express activated Kras in the pancreas and develop pancreatic intraepithelial neoplasias (PanINs), as well as those with disruption of *Aird1a* (*Ptf1a*-Cre; *Kras*^{G12D}; *Arid1a*$^{f/f}$ mice) or disruption of *Brg1* (encodes a catalytic ATPase of the SWI/SNF complex) (*Ptf1a*-Cre; *Kras*^{G12D}; *Brg1*$^{f/f}$ mice). Pancreatic ductal cells (PDCs) were isolated from *Arid1a*$^{f/f}$ mice and from *Arid1a*$^{f/f}$; SOX9OE mice, which overexpress human SOX9 upon infection with an adenovirus expressing Cre recombinase. Pancreatic tissues were collected from all mice and analyzed by histology and immunohistochemistry; cells were isolated and grown in

2-dimensional and 3-dimensional cultures. We performed microarray analyses to compare gene expression patterns in intraductal papillary mucinous neoplasms (IPMNs) from the different strains of mice. We obtained 58 samples of IPMN and 44 samples of PDAC from patients who underwent pancreatectomy in Japan, and analyzed them by immunohistochemistry.

Results: *Ptf1a*-Cre; *Kras*^{G12D} mice developed PanINs, whereas *Ptf1a*-Cre; *Kras*^{G12D}; *Arid1a*$^{f/f}$ mice developed IPMNs and PDACs; IPMNs originated from PDCs. ARID1A-deficient IPMNs did not express SOX9. ARID1A-deficient PDCs had reduced expression of SOX9 and dedifferentiated in culture. Overexpression of SOX9 in these cells allowed them to differentiate and prevented dilation of ducts. Among mice with pancreatic expression of activated Kras, those with disruption of *Arid1a* developed fewer PDACs from IPMNs than mice with disruption of *Brg1*. ARID1A-deficient IPMNs had reduced activity of the mTOR pathway. Human IPMN and PDAC specimens had reduced levels of ARID1A, SOX9, and phosphorylated S6 (a marker of mTOR pathway activation).

Levels of ARID1A correlated with levels of SOX9 and phosphorylated S6.

Conclusions: ARID1A regulates expression of SOX9, activation of the mTOR pathway, and differentiation of PDCs. ARID1A inhibits formation of PDACs from IPMNs in mice with pancreatic expression of activated KRAS, and is downregulated in IPMN and PDAC tissues from patients.

KEY WORDS: pancreatic cancer, tumorigenesis, oncogene, transcriptional regulator

351 words

Introduction

Pancreatic ductal adenocarcinoma (PDAC) is a lethal disease with an extremely poor prognosis[1]. Therefore, earlier diagnosis and more effective therapies are required to improve outcomes, which require a better understanding of the molecular mechanism of PDAC development.

Recent genome-wide sequencing studies have revealed that mutation of the subunit genes of the switch/sucrose non-fermentable (SWI/SNF) chromatin remodeling complexes are widespread across diverse human cancers[2, 3]. In fact, mutations, translocations, and deletions involving various subunits of the SWI/SNF complexes have been found in approximately 20% of human cancers, thus representing one of the most common molecular mechanisms in human cancers[2, 3]. Indeed, mutations of the subunit genes of SWI/SNF complexes have been found in 12–23% of human PDAC cases[2-4]. The SWI/SNF complexes remodel the chromatin structure using energy from ATP hydrolysis and thereby modulate gene expression[5]. Using a mouse model, we recently demonstrated that the pancreatic loss of *Brg1*, which encodes a catalytic ATPase of the SWI/SNF complex, cooperates with oncogenic *Kras* to form intraductal papillary

mucinous neoplasm (IPMN), which subsequently developed into invasive PDAC[6]. Furthermore, another study showed that *Brg1* promotes tumorigenesis in full-blown PDAC by supporting a mesenchymal-like transcriptional landscape[7]. Therefore, *Brg1* has both tumor-suppressive and oncogenic activities at distinct stages of PDAC formation.

AT-rich interactive domain 1 (ARID1A) is the most frequently mutated subunit in the SWI/SNF complexes in human PDAC[2-4, 8]. ARID1A is assumed to contribute to the specific recruitment of chromatin remodeling activity of the SWI/SNF complex by binding to transcription factors[9-12]. Furthermore, the ARID1A–DNA interaction is considered to be essential for promoter occupancy by the SWI/SNF complexes[13]. In mouse models, conditional knockout of *Arid1a* promotes ovarian tumorigenesis by activating the phosphatidylinositol 3-kinase(PI3K)/AKT/mammalian target of rapamycin (mTOR) pathway[14, 15]. Moreover, intestinal *Arid1a* deletion *per se* results in colon cancer formation in mice[16]. However, in spite of the frequent mutations of *ARID1A* in human PDAC, the *in vivo* role of *ARID1A* in pancreatic tumorigenesis remains elusive.

Therefore, in this study, we aimed to investigate the impact of *Arid1a* inactivation in the pancreas and clarify the functional role of *Arid1a* in the specification of PDAC precursors and PDAC formation in mice.

Material and Methods

Detailed methods are described in the Supplemental Materials and Methods.

Mouse lines

Experimental animals were generated by crossing *Ptf1a-Cre* (a gift from Y. Kawaguchi, Kyoto University, Kyoto, Japan)[17], *Ptf1a-Cre^{ERT2}* [18], *Hnf1b-Cre^{ERT2}* (a gift from Jorge Ferrer, Imperial College, London, UK)[19], *Kras^{G12D}* (a gift from D. Tuveson, Cold Spring Harbor Laboratory)[20], *Brg1$^{f/+}$* (a gift from D. Reisman, University of Florida, with permission from P. Chambon)[21], *Arid1a$^{f/+}$* [22], *Trp53^{R172H}* [23], and *Sox9OE* mice[24]. The mice were crossed in a mixed genetic background. All experiments were approved by the animal research committee of Kyoto University and performed in accordance with Japanese government regulations.

Pancreatic ductal cell (PDC) isolation and two-dimensional (2D) culture

PDCs were isolated following previously described protocols[25, 26]. The pancreas was minced into pieces smaller than 1 mm^3. Next, the pancreas was digested with collagenase type V for 20 min and trypsinized for 5 min;

150 trypsinization was stopped using a soy trypsin inhibitor. The cells were filtered
151 using a 40-μm cell strainer. For 2D culture, the single-cell suspension was plated
152 onto collagen-covered plates. The PDC full medium was replaced every two
153 days until the cells achieved 80% confluence. After three passages, pure ductal
154 cell lines were established.
155
156 ***Three-dimensional (3D) ductal cell culture***
157 The 3D culture of PDCs was performed according to a previously described
158 protocol[25]. PDCs were mixed with collagen and placed on top of collagen-coated
159 chamber slides. The PDC full medium was replaced every two days. PDC cysts
160 were analyzed at 7 to 11 days after plating.
161
162 ***Human samples***
163 Fifty-eight IPMN samples from 58 patients who underwent pancreatectomy
164 for IPMN or IPMN-derived PDAC at the Kyoto University Hospital from 1991 to
165 2005, and 44 PDAC samples from 44 patients who underwent pancreatectomy

166 at the Kyoto University Hospital from 2000 to 2005 were included in this study.

167 Details of the cases are summarized in Supplementary Table 1.

168

Results

Arid1a inhibits dilation of the pancreatic ducts and maintains ductal structure in adult mice

First, we examined the pattern of *Arid1a* expression in the murine pancreas, which was detected in the nuclei of all three types of pancreatic epithelial cells (ductal cells, acinar cells, and islet cells) in adult wild-type (WT) mice (Figure 1A). To investigate the functional role of *Arid1a* in pancreatic development and maintenance, we crossed the *Ptf1a-Cre* mice[17] with *Arid1a*$^{f/f}$ mice[22]. *Ptf1a-Cre; Arid1a*$^{f/f}$ mice were born according to the predicted Mendelian ratio and were indistinguishable from *Ptf1a-Cre; Arid1a*$^{f/+}$ and WT mice in appearance and body weight at 8 weeks of age (Figure 1B). Macroscopically, the *Ptf1a-Cre; Arid1a*$^{f/f}$ pancreata were indistinguishable from those of *Ptf1a-Cre; Arid1a*$^{f/+}$ and WT mice at 8 weeks of age. Histologically, ARID1A expression was not detected in the acinar cells or a subset of ductal cells in the *Ptf1a-Cre; Arid1a*$^{f/f}$ pancreata, as expected according to the Cre activity pattern in *Ptf1a-Cre* mice[17, 27]. However, at over 9 weeks of age, dilated pancreatic ducts were observed in *Ptf1a-Cre;*

185 *Arid1a*$^{f/f}$ mice. At 18 weeks of age, the dilated ducts formed cystic lesions
186 composed of *Arid1a*-deficient duct-like epithelial cells positive for cytokeratin and
187 acetylated tubulin, which are markers of PDCs (Figure 1C, 1D). These cells also
188 expressed PDX1, which is expressed in the pancreatic progenitors and islet β
189 cells in adulthood[28] (Figure 1D). This ectopic expression pattern of PDX1
190 suggested that *Arid1a* deletion results in the dedifferentiation of pancreatic
191 ductal cells. In addition, phosphorylated extracellular signal-regulated kinase
192 (pERK1/2) was detected in these cells (Figure 1D). Thus, these data indicated
193 that *Arid1a* is dispensable for pancreatic development but is required for
194 maintenance of PDCs and the structure of pancreatic ducts.
195
196 **_Ptf1a-Cre; Kras^{G12D}; Arid1a$^{f/f}$_ mice develop multilocular fluid-filled cystic**
197 **neoplasms**
198 To investigate the role of *Arid1a* in pancreatic tumorigenesis, we crossed
199 *Ptf1a-Cre; Arid1a*$^{f/f}$ mice with *loxp-stop-loxp Kras*^{G12D} (*Kras*^{G12D}) mice. Similar to
200 *Ptf1a-Cre; Kras*^{G12D} mice[20], *Ptf1a-Cre; Kras*^{G12D}*; Arid1a*$^{f/+}$ mice developed

pancreatic intraepithelial neoplasias (PanIN) throughout the pancreata. In contrast, *Ptf1a-Cre; Kras^{G12D}; Arid1a$^{f/f}$* mice developed multilocular fluid-filled cysts throughout the pancreata by 9 weeks of age (Figure 2A), and the pancreata were enlarged due to the extensive cystic lesions (Figure 2B). Histologically, the cystic lesions were composed of dysplastic cells with abundant supranuclear mucin (Figure 2C). Immunohistochemical analysis revealed that the epithelial cells of the neoplastic cysts observed in *Ptf1a-Cre; Kras^{G12D}; Arid1a$^{f/f}$* mice were positive for cytokeratin and acetylated tubulin[29] and negative for amylase expression (Figure 2C), indicating that these neoplastic cells showed a duct-like character. In addition, the absence of ARID1A expression and activation of the mitogen-activated protein kinase (MAPK) cascade were observed in these neoplastic cells, as expected (Figure 2D). The proliferation activity was low in the cystic neoplasms based on the low positive rate of Ki67 expression compared to that of the PanIN in *Ptf1a-Cre; Kras^{G12D}* mice (Figure 2D), suggesting that expansion of the cystic neoplasms is not due to aggressive cell growth but is most likely due to abundant intraductal mucin.

Moreover, acinar-to-ductal metaplasia (ADM) and PanIN were also observed in *Ptf1a-Cre; Kras^{G12D}; Arid1a$^{f/f}$* mice (Supplementary Figure 1), suggesting that absence of *Arid1a* expression does not inhibit PanIN formation. Thus, these results indicated that deletion of *Arid1a* with mutant *Kras* results in formation of cystic neoplasms in the pancreas.

Cystic neoplasms in *Ptf1a-Cre; Kras^{G12D}; Arid1a$^{f/f}$* mice resemble human IPMN but not mucinous cystic neoplasms (MCN)

There are two types of pancreatic mucus-producing cystic neoplasms in humans: IPMN and MCN[30]. IPMN are characterized by connection to the pancreatic ductal system, whereas MCN are characterized by dense ovarian-like stroma[30, 31]. Given that the cystic neoplasms in *Ptf1a-Cre; Kras^{G12D}; Arid1a$^{f/f}$* mice had abundant mucin, we investigated whether these cystic neoplasms more closely resembled human IPMN or MCN. Histological examination revealed that the cystic neoplasms were connected to the pancreatic ductal system (Figure 2C) and lacked ovarian-like stroma, as indicated by staining for

estrogen receptor and progesterone receptor (Supplementary Figure 2). In addition, most of the cystic neoplasms lacked the MCN-typical dense stroma exhibiting wavy nuclei. These findings indicated that the cystic neoplasms in *Ptf1a-Cre; Kras^{G12D}; Arid1a$^{f/f}$* mice resembled human IPMN but not MCN. Human IPMN can be further classified into four types according to the directions of differentiation of the neoplastic cells and mucin expression patterns: gastric, intestinal, pancreatobiliary, and oncocytic type[31, 32]. The IPMN-like cells expressed MUC1 and MUC5AC but lacked MUC2 expression in *Ptf1a-Cre; Kras^{G12D}; Arid1a$^{f/f}$* mice, indicating that the mucin expression pattern was similar to that of human pancreatobiliary- or oncocytic-type IPMN (Figure 2E).

Molecular characterization of IPMN-like cystic neoplasms

Because human IPMN represent a form of PDAC precursor lesions, we examined certain markers of the signaling pathways known to play a critical role in pancreatic carcinogenesis. Phospho-STAT3, which is a critical signaling pathway for PDAC formation[33], was upregulated in the IPMN of *Ptf1a-Cre;*

Kras^{G12D}; Arid1a$^{f/f}$ mice but was weaker than the phospho-STAT3 expression detected in the PanIN of *Ptf1a-Cre; Kras^{G12D}* mice (Supplementary Figure 3A). PDX1 expression was positive in the mouse IPMN (Supplementary Figure 3B). The expression levels of p21, p16 (INK4A), and p53 were reduced or completely absent in the IPMN of *Ptf1a-Cre; Kras^{G12D}; Arid1a$^{f/f}$* mice, as observed in *Ptf1a-Cre; Kras^{G12D}; Brg1$^{f/f}$* mice[6], whereas SMAD4 expression was maintained in the *Arid1a*-deficient IPMN (Supplementary Figure 3C–F).

Mouse IPMN gradually develop into PDAC

A previous report indicated that the IPMN in *Ptf1a-Cre; Kras^{G12D}; Brg1$^{f/f}$* mice frequently progressed to PDAC by 18 weeks of age[6]. Similar to these mice, at 18 weeks of age, the *Ptf1a-Cre; Kras^{G12D}; Arid1a$^{f/f}$* mice developed IPMN with varying grades of dysplasia (Figure 3A); however, PDAC was not observed (n = 13). Even at 24 weeks of age, PDAC did not develop in *Ptf1a-Cre; Kras^{G12D}; Arid1a$^{f/f}$* mice (n = 15). At 48 weeks of age, PDAC developed in 3 of 15 (20%) *Ptf1a-Cre; Kras^{G12D}; Arid1a$^{f/f}$* mice (Figure 3B, C), one of which was carcinoma

265 *in situ*, and the others were invasive adenocarcinoma (Figure 3C).
266 Immunohistochemical analysis revealed that the PDAC cells in *Ptf1a-Cre;*
267 *Kras^{G12D}; Arid1a$^{f/f}$* mice were negative for ARID1A and positive for pERK1/2
268 expression, as expected. The frequent positive expression of Ki67 indicated
269 vigorous growth of the PDAC cells, and PDX1 expression was detected in the
270 PDAC cells (Figure 3D). Given that the incidence of PDAC formation in
271 *Ptf1a-Cre; Kras^{G12D}* and *Pdx1-Cre; Kras^{G12D}* mice was previously estimated to
272 be less than 10% around 50 weeks of age[20] and that no PDAC was observed in
273 our control *Ptf1a-Cre; Kras^{G12D}* (n = 8) and *Ptf1a-Cre; Kras^{G12D}; Arid1a$^{f/+}$* (n = 16)
274 mice at 44–48 weeks of age (Figure 3B), these data suggested that *Arid1a*
275 inhibits IPMN-derived PDAC formation and functions as a tumor suppressor in
276 the murine pancreas.

277 Although deletion of *Arid1a* promotes IPMN and IPMN-derived PDAC
278 formation, there was no significant difference in survival between *Ptf1a-Cre;*
279 *Kras^{G12D}; Arid1a$^{f/+}$* and *Ptf1a-Cre; Kras^{G12D}; Arid1a$^{f/f}$* mice (Supplementary
280 Figure 4). This was most likely due to the slow progression of PDAC from

Arid1a-deficient IPMN.

Moreover, we performed immunohistochemical staining of ARID1A in PanIN-derived PDAC sections from *Ptf1a-Cre; Kras^{G12D}; Trp53^{R172H}* (KPC) mice (n = 8), and found positive ARID1 expression in all sections examined (data not shown).

Mouse IPMN originate from PDCs but not from pancreatic acinar cells

Although PanIN showed a duct-like characteristic, studies with mouse models have shown that the cellular origin of PanIN is the acinar compartment[34, 35]. Moreover, the cellular origin of human IPMN has been considered to be the ductal compartment, because human IPMN are found in ductal structures. In some mouse models, the cellular origin of IPMN was reported to be the ductal compartment or duct glands[6, 36]. To investigate the cellular origin of mouse *Arid1a*-deficient IPMN, we used two tamoxifen-inducible Cre lines, *Ptf1a-Cre^{ERT2}* and *Hnf1b-Cre^{ERT2}*, which enabled Cre recombination in adult pancreatic acinar cells and PDC with tamoxifen treatment, respectively[19, 35]. First, we crossed

297 *Ptf1a-Cre^{ERT2}* mice with *Kras^{G12D}; Arid1a$^{f/f}$* mice (Figure 4A). *Ptf1a-Cre^{ERT2}; Kras^{G12D}; Arid1a$^{f/+}$* and *Ptf1a-Cre^{ERT2}; Kras^{G12D}; Arid1a$^{f/f}$* mice were treated with tamoxifen and caerulein and were examined as presented in Figure 4B. Both mouse lines developed multiple PanIN but no IPMN (Figure 4C). This indicated that *Arid1a* is not required for PanIN formation from acinar cells and that the acinar compartment is not the cellular origin of IPMN in this mouse model.

We next crossed *Hnf1b-Cre^{ERT2}* mice with *Kras^{G12D}; Arid1a$^{f/f}$* mice (Figure 4D). *Hnf1b-Cre^{ERT2}; Kras^{G12D}; Arid1a$^{f/+}$* and *Hnf1b-Cre^{ERT2}; Kras^{G12D}; Arid1a$^{f/f}$* mice were treated with tamoxifen and examined as presented in Figure 4E. Although *Hnf1b-Cre^{ERT2}; Kras^{G12D}; Arid1a$^{f/+}$* mice showed no signs of duct atypia, atypical PDCs were observed in all three *Hnf1b-Cre^{ERT2}; Kras^{G12D}; Arid1a$^{f/f}$* mice. Furthermore, one of the six *Hnf1b-Cre^{ERT2}; Kras^{G12D}; Arid1a$^{f/f}$* mice developed cystic lesions composed of a single layer of columnar cells with supranuclear mucin. We observed the absence of expression and activation of the MAPK cascade in the epithelial cells of these cystic lesions (Figure 4F). The mucin expression pattern of the cystic lesions in *Hnf1b-Cre^{ERT2}; Kras^{G12D}; Arid1a$^{f/f}$* mice

313 was similar to that of the IPMN in *Ptf1a-Cre; Kras^{G12D}; Arid1a$^{f/f}$* mice (Figure 4F).
314 These data indicated that *Arid1a* inhibits the dysplasia of adult PDCs and IPMN
315 transformation from adult PDCs in the context of activated KRAS.
316
317 **_Arid1a_ loss leads to the dedifferentiation of PDCs and pancreatic ductal**
318 **dilation via suppression of SOX9 expression**
319 To determine the underlying molecular mechanism by which IPMN are
320 formed from PDCs in the absence of *Arid1a*, we performed immunostaining for
321 SOX9, a key transcriptional factor for the differentiation of PDCs[37, 38]. Notably,
322 immunohistochemical analysis revealed that SOX9 expression was absent in
323 the dilated ducts of *Ptf1a-Cre; Arid1a$^{f/f}$* mice and in the IPMN of *Ptf1a-Cre;*
324 *Kras^{G12D}; Arid1a$^{f/+}$* and *Hnf1b-Cre^{ERT2}; Kras^{G12D}; Arid1a$^{f/f}$* mice (Figure 5A). Thus,
325 we hypothesized that the neoplastic transformation of PDCs was mediated by
326 the downregulation of SOX9 expression in the absence of *Arid1a*. To test this
327 hypothesis, we isolated and cultured PDCs from *Arid1a$^{f/f}$* mice[25, 26], and then
328 induced genetic recombination by infecting the PDCs with an adenovirus

329 expressing both Cre recombinase and GFP (Ad-Cre). We used an adenovirus
330 expressing GFP (Ad-GFP) as a control (Figure 5B). Ad-Cre-infected PDCs
331 showed markedly lower expression levels of *Arid1a*, as expected, and formed
332 cysts of significantly larger size in 3D culture than control Ad-GFP-infected PDCs
333 isolated from the same mouse (Figure 5C, 5E). Furthermore, Ad-Cre-infected
334 PDCs exhibited lower expression levels of mouse *Sox9* (*mo-Sox9*) and higher
335 expression levels of pancreatic progenitor markers, including *Gata4* and *Gata6*,
336 than control PDCs (Figure 5E). These findings indicated that loss of *Arid1a*
337 expression in PDCs results in suppression of *Sox9* expression, dedifferentiation
338 of PDCs, and disturbance of the pancreatic ductal structure *ex vivo*.

339 To investigate whether these effects of *Arid1a* deficiency in PDCs were due
340 to suppression of SOX9 expression, we next isolated and cultured PDCs from
341 *Arid1a*$^{f/f}$*; Sox9OE* mice in which *Arid1a* was deleted and human *Sox9* (*hu-Sox9*)
342 was simultaneously overexpressed after Cre recombination. We then induced
343 genetic recombination by Cre recombinase, similar to the procedure described
344 above for *Arid1a*$^{f/f}$ mice (Figure 5B). Ad-Cre-infected PDCs from *Arid1a*$^{f/f}$*;*

345 *Sox9OE* mice showed lower expression levels of *Arid1a* and *mo-Sox9* but
346 extremely higher expression levels of *hu-Sox9* than the control cells, as
347 expected (Figure 5E). Notably, these *Arid1a*-deficient and *Sox9*-overexpressed
348 PDCs expressed equal levels of pancreatic progenitor markers, including *Gata4*
349 and *Gata6*, and formed cysts of equal size in 3D culture compared to WT control
350 PDCs (Figure 5D, 5E). These data indicated that overexpression of *Sox9*
351 canceled out the effect of *Arid1a* deletion on the dedifferentiation of PDCs and
352 ductal dilation *ex vivo*.

353 To investigate whether the effects of *Arid1a* deletion in PDCs on pancreatic
354 ductal dilation were mediated by downregulation of SOX9 expression *in vivo*, we
355 next generated *Ptf1a-Cre; Arid1a$^{f/f}$; Sox9OE* mice. Histologically, pancreatic
356 ductal dilation was not observed in *Ptf1a-Cre; Arid1a$^{f/f}$; Sox9OE* mice at 9-20
357 weeks of age (n = 3) (Supplementary Figure 5A, C), indicating that Sox9
358 overexpression offsets the effect of *Arid1a* deletion on ductal dilation *in vivo*.

359 To investigate whether Sox9 overexpression also prevents development of
360 IPMN from *Arid1a*-deficient PDCs *in vivo*, we next generated *Ptf1a-Cre;*

Kras^{G12D}; Arid1a$^{f/f}$; Sox9OE mice. At 4-8 weeks of age, IPMN was formed in *Ptf1a-Cre; Kras^{G12D}; Arid1a$^{f/f}$; Sox9OE* mice (n = 4) similarly to *Ptf1a-Cre; Kras^{G12D}; Arid1a$^{f/f}$* mice (Supplementary Figure 5B, C), indicating that only Sox9 overexpression does not cancel out the effect of combination of *Arid1a* deletion and oncogenic *Kras* in terms of IPMN development. Therefore, we concluded that *Arid1a* prevents the dedifferentiation of PDCs and maintains the pancreatic ductal structure through regulation of *Sox9* expression *in vivo*.

Furthermore, we performed a global microarray analysis of *Arid1a*-deficient PDCs to investigate the specific pathways affected by *Arid1a* deletion in PDCs, leading to IPMN development. The pathway analysis revealed that Ras-associated pathways (the Ras signaling pathway and PI3K-AKT signaling pathway) were most strongly affected by *Arid1a* deletion in PDCs. Moreover, GO enrichment analysis revealed that genes encoding membrane proteins were suppressed by *Arid1a* loss (Supplementary Figure 6). Therefore, these pathways might also play roles in the development of IPMN from *Arid1a*-deficient PDCs.

The mTOR pathway is activated during the progression of IPMN to PDAC

Although IPMN was generally formed in *Ptf1a-Cre; Kras^{G12D}; Arid1a$^{f/f}$* mice, similar to *Ptf1a-Cre; Kras^{G12D}; Brg1$^{f/f}$* mice at the same age, the incidence of PDAC formation was much lower in the *Ptf1a-Cre; Kras^{G12D}; Arid1a$^{f/f}$* mice compared with that in *Ptf1a-Cre; Kras^{G12D}; Brg1$^{f/f}$* mice[6]. BRG1 expression was observed in the IPMN of *Ptf1a-Cre; Kras^{G12D}; Arid1a$^{f/f}$* mice, whereas ARID1A expression was retained in the IPMN of *Ptf1a-Cre; Kras^{G12D}; Brg1$^{f/f}$* mice (Figure 6A), indicating that BRG1 and ARID1A expression are independently regulated in the absence of *Arid1a* and *Brg1*, respectively.

To better understand the mechanism driving the progression of IPMN to PDAC in the absence of *Arid1a*, we next compared the gene expression patterns between *Ptf1a-Cre; Kras^{G12D}; Arid1a$^{f/f}$* and *Ptf1a-Cre; Kras^{G12D}; Brg1$^{f/f}$* mice. We performed microarray analysis of mRNA obtained from the IPMN in mice of these two genotypes by laser micro-dissection. GSEA[39, 40] revealed that seven gene sets associated with Notch, the PRC2 complex, mTOR pathway,

KRAS, and embryonic stem cells were differentially expressed in *Arid1a*-deficient IPMN compared to *Brg1*-deficient IPMN (Figure 6B, Supplementary Figure 7). Although mutations in the mTOR pathway have not been commonly observed in human PDAC[41, 42], this pathway, which can be activated by Kras, is important for growth, metastasis, and chemotherapy tolerance during PDAC[43-46]. To validate the correlative relationship between *Arid1a* expression and the mTOR pathway in the IPMN of these mice, we next performed immunohistochemistry for pS6 at serine 235/236. Consistent with the microarray data, pS6 was barely expressed in the *Arid1a*-deficient IPMN, whereas pS6 was strongly expressed in the *Brg1*-deficient IPMN (Figure 6C). Notably, pS6 was expressed in IPMN-derived *Arid1a*-deficient PDAC (Figure 6C), indicating that the mTOR signaling pathway is activated during the progression of IPMN to PDAC in *Ptf1a-Cre; Kras^{G12D}; Arid1a$^{f/f}$* mice. These results suggested that the mTOR signaling pathway appears to be a key signaling pathway for the progression of IPMN to PDAC in the absence of *Arid1a* *in vivo.* Moreover, the lower frequency of PDAC formation could be attributed to

409 the lower activity of the mTOR signaling pathway in *Arid1a*-deficient IPMN
410 compared to *Brg1*-deficient IPMN.

411 Next, we investigated whether *Arid1a* deletion could alter the mTOR pathway
412 activity in PDCs *ex vivo*. PDCs isolated from *Arid1a*$^{f/f}$ mice were transfected with
413 Ad-GFP and Ad-Cre as shown in Figure 5B. qPCR analysis revealed that
414 expression levels of *Pik3ca, Akt3*, and *mTor* were downregulated in
415 *Arid1a*-deficient PDCs compared with the control, indicating that *Arid1a*
416 regulates activity of the mTOR pathway by supporting the expression of
417 components of this pathway in PDCs (Figure 6D).

418

419 **Absence of ARID1A expression in subsets of human IPMN and PDAC**

420 Mutations of *ARID1A* are frequently observed In human PDAC[2-4, 8].
421 Therefore, we next examined ARID1A expression in human IPMN and PDAC
422 samples. Immunohistochemical analysis revealed that ARID1A expression was
423 absent in 13 out of 58 surgically resected human IPMN samples and in 16 out of
424 44 surgically resected human PDAC samples (Figure 7A, Supplementary Table

1). As presented in Supplementary Table 1, patients with ARID1A-negative IPMN were indistinguishable from those with ARID1A-positive IPMN with respect to sex, age, clinical subtype, and incidence of PDAC. The frequency of oncocytic-type IPMN was significantly higher and that of gastric-type IPMN was significantly lower in cases of ARID1A-negative IPMN than in cases of ARID1A-positive IPMN.

Given that *Arid1a* deletion resulted in the suppression of *Sox9* expression in our mouse model, we further examined the correlation between ARID1A and SOX9 expression in human IPMN (Figure 7A, Supplementary Table 1). Thirty-eight percent of the ARID1A-negative human IPMN samples (5/13) were positive for SOX9, whereas 84.4% of the ARID1A-positive IPMN samples (38/45) were positive for SOX9. Similarly, 56.3% of the ARID1A-negative PDAC samples (9/16) were positive for SOX9, whereas 96.4% of the ARID1A-positive PDAC samples (27/28) were positive for SOX9 (Supplementary Table 1). Thus, absence of ARID1A expression was observed in subsets of human IPMN and PDAC, and a significant positive correlation was observed between the

441 expression of ARID1A and SOX9 in human IPMN and PDAC.

442 To examine whether activity of the mTOR pathway was associated with
443 ARID1A expression in human IPMN and PDAC, we next performed
444 immunohistochemistry for pS6. We found a significant positive correlation
445 between the expression of ARID1A and pS6 in human IPMN: pS6 was observed
446 in 30% of the ARID1A-negative human IPMN samples (4/13), whereas it was
447 expressed in 66.7% of the ARID1A-positive human IPMN samples (30/45)
448 (Figure 7A, Supplementary Table 1). Similarly, 37.5% of the ARID1A-negative
449 PDAC samples (6/16) were positive for pS6, whereas 60.7% of the
450 ARID1A-positive PDAC samples (17/28) were positive for pS6 (Supplementary
451 Table 1). Thus, activation of the mTOR pathway appears to be reduced in cases
452 of ARID1A-negative human IPMN and PDAC.

453 Furthermore, consistent with the mouse data, publicly available mRNA
454 expression data of human PDAC from The Cancer Genome Atlas (TCGA)
455 revealed that the level of *ARID1A* expression is closely correlated with that of the
456 components of the mTOR pathway, including *mTOR*, *PIK3CA*, *AKT3*, and

457 *RICTOR* (Spearman rank correlation coefficient = 0.63, 0.556, 0.463, 0.501,
458 respectively; Figure 7B, C). These data further support the conclusion that
459 ARID1A regulates mTOR pathway activity by supporting the expression of
460 components of the mTOR pathway in human PDAC.
461

Discussion

Recent genome-wide sequencing studies have revealed that human PDAC mutations are classified into ten core signaling pathways[47]. The SWI/SNF chromatin remodeling complex is one of these pathways, and 12–23% of all human PDACs show inactivated mutations in the SWI/SNF complexes, [2-4, 47] including *ARID1A* as the most frequently mutated gene[2-4, 8]. However, the mechanism by which *ARID1A* inactivation contributes to pancreatic tumorigenesis *in vivo* remains unknown. In the present study, we revealed five novel findings about the role of *Arid1a* in pancreatic tumorigenesis in mice.

First, we showed that pancreatic *Arid1a* deletion collaborates with mutant *Kras* to form IPMN and IPMN-derived PDAC, demonstrating that *Arid1a* acts as a tumor suppressor in the murine pancreas in the presence of mutant *Kras*. Similarly, we previously showed that the pancreatic loss of *Brg1*, encoding the ATPase subunit of the SWI/SNF complex, results in formation of IPMN and IPMN-derived PDAC in the presence of mutant *Kras*[6]. *Arid1a*-deficient IPMN had similar histological features with *Brg1*-deficient IPMN. These findings suggested

478 that *Arid1a* and *Brg1* cooperate to suppress IPMN formation in the murine
479 pancreas. Mechanistically, our findings, together with those of previous studies,
480 suggest that *Arid1a* and *Brg1* inhibit the dedifferentiation of PDCs and thus
481 IPMN formation through regulation of genes that sustain pancreatic duct cell
482 identity, including *Sox9*[7]. In contrast, *Brg1* was shown to promote tumorigenesis
483 in full-blown PDAC by supporting a mesenchymal-like transcriptional landscape[7].
484 Therefore, similar to transforming growth factor-beta and Wnt signaling[48, 49],
485 BRG1 plays both tumor-suppressive and promotive functions at distinct stages
486 of PDAC in a context-dependent manner. In line with the context-dependent
487 roles of BRG1 in PDAC, loss of *Brg1* shows opposing effects on the progression
488 of lung cancer at distinct stages of the disease[50]. Furthermore, our data suggest
489 that *Arid1a* appears to have a tumor-promotive function in established IPMN
490 through positive regulation of the mTOR pathway. These context-dependent
491 roles of the SWI/SNF complex are most likely due to their multiple cellular
492 functions regulated by a wide range of target genes. Of interest, a recent study
493 demonstrated that patients with ARID1A-negative PDAC had a better prognosis

494 with respect to survival compared to those with ARID1A-positive PDAC[8].
495 Therefore, future studies are required to clarify precisely how *Arid1a* inactivation
496 contributes to the progression of established PDAC *in vivo*.

497 Second, regarding the cellular origin of IPMNs, we showed that mouse
498 *Arid1a*-deficient IPMN originate from the ductal compartment but not from the
499 acinar compartment. In line with this finding, the cellular origin of mouse
500 *Brg1*-deficient IPMN was reported to be the PDCs[6]. However, a recent study
501 showed that the cellular origin of mouse IPMN induced by loss of trefoil factor
502 family 2 (TFF2) was pancreatic duct gland (PDG) cells[36]. Given that enlargement
503 of PDGs was not observed in the *Ptf1a-Cre; Kras^{G12D}; Arid1a$^{f/f}$* mice and that the
504 expression of SMAD4, which is essential for the IPMN suppressive role of TFF2
505 [36, 51], was maintained in the *Arid1a*-deficient IPMNs, the present study suggests
506 that the IPMN induced by loss of *Arid1a* or *Brg1* have a different cellular origin
507 from those induced by the loss of *Smad4*/*Tff2*.

508 Third, we showed that *Arid1a* suppresses the dedifferentiation of PDCs and
509 thus the formation of IPMN from PDCs in part through positive regulation of

510 *Sox9* expression, which is required for ductal cell differentiation and
511 maintenance[39]. Consistent with our results, *Brg1* inhibited the dedifferentiation of
512 PDCs and IPMN formation through regulation of *Sox9* expression. When *Sox9*
513 was inactivated during the embryonic period, a complete tissue-penetrating
514 pancreatic cystic phenotype was observed. Similar to embryonic inactivation,
515 conditional *Sox9* deletion in adult mice resulted in a polycystic pancreas[39].
516 Therefore, *Sox9* appears to be one of the key downstream effectors of the
517 SIW/SNF complex in maintenance of the pancreatic ductal structure to inhibit the
518 development of IPMN from PDCs.

519 Fourth, we found that activity of the mTOR pathway is relatively lower in
520 *Arid1a*-deficient IPMN compared to *Brg1*-deficient IPMN. The mTOR pathway
521 promotes pancreatic carcinogenesis[43-46]. Recenty, Kopp JL et al. reported that
522 activation of Kras and AKt-mTor pathway leads to IPMN and PDAC formation [52].
523 This is in line with the finding that the incidence of PDAC formation in
524 *Ptf1a-CreKras^{G12D}; Arid1a$^{f/f}$* mice was markedly lower than that in *Ptf1a-Cre;*
525 *Kras^{G12D}; Brg1$^{f/f}$* mice despite the histological similarities between

526 *Arid1a*-deficient and *Brg1*-deficient IPMN. Thus, activation of the mTOR
527 pathway appears to be important for the progression to PDAC from IPMN in the
528 absence of *Arid1a*.

529 Finally, we found that ARID1A expression is absent in subsets of human IPMN
530 and PDAC. Furthermore, we found a positive correlation between the expression
531 of ARID1A and SOX9/components of the mTOR pathway in human IPMN and
532 PDCA. Considering the strong correlation between ARID1A and the mTOR
533 pathway in human PDAC, the expression level of ARID1A might affect the
534 effectiveness of mTOR inhibitors for human PDAC. In addition, synthetic lethality
535 of *Arid1a*-mutated cancers was recently demonstrated by targeting EZH2 or ATR.
536 Therefore, it would be of value to investigate whether EZH2 or ATR might be
537 effective for the treatment of ARID1A-negative PDAC. Although we showed that
538 AIRD1A expression is absent in subsets of human IPMN and revealed that the
539 loss of ARID1A contributes to pancreatic tumorigenesis in this study, it remains
540 unclear precisely how ARID1A expression is reduced or lost in human IPMN.
541 Therefore, future studies are required to clarify the underlying mechanism.

In conclusion, we revealed that *Arid1a* inhibits duct cell-derived IPMN and subsequent PDAC formation in the context of oncogenic *Kras*, demonstrating a tumor-suppressive role of *Arid1a* in the pancreas *in vivo*. *Arid1a* prevents the dedifferentiation of PDCs and maintains pancreatic ductal structure in part through regulation of *Sox9* expression, providing mechanistic insight into IPMN formation. Expression of ARID1A and SOX9/components of the mTOR pathway was positively correlated in human IPMN and PDCA. Our data point to *Arid1a* as a cell-type specific mediator of *Kras*-driven tumorigenesis in the pancreas and underscore that the SWI/SNF chromatin remodeling complex is a critical determinant for the distinct route of PDAC formation.

Acknowledgements

The authors thank Yoshiya Kawaguchi for sharing the *Ptf1a-Cre* mice.

References

1. Hidalgo M, Cascinu S, Kleeff J, et al. Addressing the challenges of pancreatic cancer: future directions for improving outcomes. Pancreatology 2015;15:8-18.

2. Shain AH, Pollack JR. The spectrum of SWI/SNF mutations, ubiquitous in human cancers. PLoS One 2013;8:e55119.

3. **Kadoch C**, **Hargreaves DC**, Hodges C, et al. Proteomic and bioinformatic analysis of mammalian SWI/SNF complexes identifies extensive roles in human malignancy. Nat Genet 2013;45:592-601.

4. **Witkiewicz AK**, **McMillan EA**, **Balaji U**, et al. Whole-exome sequencing of pancreatic cancer defines genetic diversity and therapeutic targets. Nat Commun 2015;6:6744.

5. Wilson BG, Roberts CW. SWI/SNF nucleosome remodellers and cancer. Nat Rev Cancer 2011;11:481-92.

6. von Figura G, Fukuda A, Roy N, et al. The chromatin regulator Brg1 suppresses formation of intraductal papillary mucinous neoplasm and pancreatic ductal adenocarcinoma. Nat Cell Biol 2014;16:255-67.

7. **Roy N**, **Malik S**, Villanueva KE, et al. Brg1 promotes both tumor-suppressive and oncogenic activities at distinct stages of pancreatic cancer formation. Genes Dev 2015;29:658-71.

8. Sausen M, Phallen J, Adleff V, et al. Clinical implications of genomic alterations in the tumour and circulation of pancreatic cancer patients. Nat Commun 2015;6:7686.

9. Wu JN, Roberts CW. ARID1A mutations in cancer: another epigenetic tumor suppressor? Cancer Discov 2013;3:35-43.

10. Dallas PB, Cheney IW, Liao DW, et al. p300/CREB binding protein-related protein p270 is a component of mammalian SWI/SNF complexes. Mol Cell Biol 1998;18:3596-603.

11. Nie Z, Xue Y, Yang D, et al. A specificity and targeting subunit of a human SWI/SNF family-related chromatin-remodeling complex. Mol Cell Biol 2000;20:8879-88.

12. Trotter KW, Archer TK. Reconstitution of glucocorticoid receptor-dependent transcription in vivo. Mol Cell Biol 2004;24:3347-58.

13. Chandler RL, Brennan J, Schisler JC, et al. ARID1a-DNA interactions are required for promoter occupancy by SWI/SNF. Mol Cell Biol 2013;33:265-80.

14. Guan B, Rahmanto YS, Wu RC, et al. Roles of deletion of Arid1a, a tumor suppressor, in mouse ovarian tumorigenesis. J Natl Cancer Inst 2014;106.

15. **Chandler RL**, **Damrauer JS**, Raab JR, et al. Coexistent ARID1A-PIK3CA mutations promote ovarian clear-cell tumorigenesis through pro-tumorigenic inflammatory cytokine signalling. Nat Commun 2015;6:6118.

16. Mathur R, Alver BH, San Roman AK, et al. ARID1A loss impairs enhancer-mediated gene regulation and drives colon cancer in mice. Nat Genet 2017;49:296-302.

17. Kawaguchi Y, Cooper B, Gannon M, et al. The role of the transcriptional regulator Ptf1a in converting intestinal to pancreatic progenitors. Nat Genet 2002;32:128-34.

18. Pan FC, Bankaitis ED, Boyer D, et al. Spatiotemporal patterns of multipotentiality in Ptf1a-expressing cells during pancreas organogenesis and injury-induced facultative restoration. Development 2013;140:751-64.

19. **Solar M**, **Cardalda C**, **Houbracken I**, et al. Pancreatic exocrine duct cells give rise to insulin-producing beta cells during embryogenesis but not after birth. Dev Cell 2009;17:849-60.

20. Hingorani SR, Petricoin EF, Maitra A. Preinvasive and invasive ductal pancreatic cancer and its early detection in the mouse. Cancer Cell 2003;4:437-450.

21. Sumi-Ichinose C, Ichinose H, Metzger D, et al. SNF2beta-BRG1 is essential for the viability of F9 murine embryonal carcinoma cells. Mol Cell Biol 1997;17:5976-86.

22. Gao X, Tate P, Hu P, et al. ES cell pluripotency and germ-layer formation require the SWI/SNF chromatin remodeling component BAF250a. Proc Natl Acad Sci U S A 2008;105:6656-61.

23. **Li B**, **Murphy L**, Laucirica R. A transgenic mouse model for mammary

carcinogenesis. oncogene 1998;16:997-1007.

24. Kim Y, Murao H, Yamamoto K, et al. Generation of transgenic mice for conditional overexpression of Sox9. J Bone Miner Metab 2011;29:123-9.

25. Reichert M, Takano S, Heeg S, et al. Isolation, culture and genetic manipulation of mouse pancreatic ductal cells. Nat Protoc 2013;8:1354-65.

26. Reichert M, Rhim AD, Rustgi AK. Culturing primary mouse pancreatic ductal cells. Cold Spring Harb Protoc 2015;2015:558-61.

27. Heiser PW, Lau J, Taketo MM, et al. Stabilization of beta-catenin impacts pancreas growth. Development 2006;133:2023-32.

28. **Ahlgren U**, **Jonsson J**, Jonsson L, et al. β-cell-specific inactivation of the mouse Ipf1/Pdx1 gene results in loss of the beta-cell phenotype and maturity onset diabetes. Genes Dev 1998;12:1763-8.

29. Seeley ES, Carriere C, Goetze T, et al. Pancreatic cancer and precursor pancreatic intraepithelial neoplasia lesions are devoid of primary cilia. Cancer Res 2009;69:422-30.

30. **Matthaei H**, **Schulick RD**, **Hruban RH**, et al. Cystic precursors to invasive pancreatic cancer. Nat Rev Gastroenterol Hepatol 2011;8:141-50.

31. Shi C, Hruban RH. Intraductal papillary mucinous neoplasm. Hum Pathol 2012;43:1-16.

32. Takasu N, Kimura W, Moriya T, et al. Intraductal papillary-mucinous neoplasms of the gastric and intestinal types may have less malignant potential than the pancreatobiliary type. Pancreas 2010;39:604-10.

33. **Fukuda A**, **Wang SC**, Morris JPt, et al. Stat3 and MMP7 contribute to pancreatic ductal adenocarcinoma initiation and progression. Cancer Cell 2011;19:441-55.

34. Habbe N, Shi G, Meguid RA, et al. Spontaneous induction of murine pancreatic intraepithelial neoplasia (mPanIN) by acinar cell targeting of oncogenic Kras in adult mice. Proc Natl Acad Sci U S A 2008;105:18913-8.

35. **Kopp JL**, **von Figura G**, Mayes E, et al. Identification of Sox9-dependent

acinar-to-ductal reprogramming as the principal mechanism for initiation of pancreatic ductal adenocarcinoma. Cancer Cell 2012;22:737-50.

36. Yamaguchi J, Mino-Kenudson M, Liss AS, et al. Loss of Trefoil Factor 2 From Pancreatic Duct Glands Promotes Formation of Intraductal Papillary Mucinous Neoplasms in Mice. Gastroenterology 2016;151:1232-1244 e10.

37. **Delous M**, **Yin C**, **Shin D**, et al. Sox9b is a key regulator of pancreaticobiliary ductal system development. PLoS Genet 2012;8:e1002754.

38. Shih HP, Kopp JL, Sandhu M, et al. A Notch-dependent molecular circuitry initiates pancreatic endocrine and ductal cell differentiation. Development 2012;139:2488-99.

39. Subramanian A, Tamayo P, Mootha VK, et al. Gene set enrichment analysis: a knowledge-based approach for interpreting genome-wide expression profiles. Proc Natl Acad Sci U S A 2005;102:15545-50.

40. Mootha VK, Lindgren CM, Eriksson KF, et al. PGC-1alpha-responsive

669 genes involved in oxidative phosphorylation are coordinately
670 downregulated in human diabetes. Nat Genet 2003;34:267-73.
671 41. Okami K, Wu L, Riggins G, et al. Analysis of PTEN/MMAC1 alterations in
672 aerodigestive tract tumors. Cancer Res 1998;58:509-11.
673 42. Samuels Y, Velculescu VE. Oncogenic mutations of PIK3CA in human
674 cancers. Cell Cycle 2004;3:1221-4.
675 43. Asano T, Yao Y, Zhu J, et al. The PI 3-kinase/Akt signaling pathway is
676 activated due to aberrant Pten expression and targets transcription
677 factors NF-kappaB and c-Myc in pancreatic cancer cells. Oncogene
678 2004;23:8571-80.
679 44. Asano T, Yao Y, Zhu J, et al. The rapamycin analog CCI-779 is a potent
680 inhibitor of pancreatic cancer cell proliferation. Biochem Biophys Res
681 Commun 2005;331:295-302.
682 45. Lim KH, Counter CM. Reduction in the requirement of oncogenic Ras
683 signaling to activation of PI3K/AKT pathway during tumor maintenance.
684 Cancer Cell 2005;8:381-92.

46. **Bruns CJ**, **Koehl GE**, Guba M, et al. Rapamycin-induced endothelial cell death and tumor vessel thrombosis potentiate cytotoxic therapy against pancreatic cancer. Clin Cancer Res 2004;10:2109-19.

47. Bailey P, Chang DK, Nones K, et al. Genomic analyses identify molecular subtypes of pancreatic cancer. Nature 2016;531:47-52.

48. Ikushima H, Miyazono K. TGFβ signalling: a complex web in cancer progression. Nat Rev Cancer 2010;10:415-424.

49. John P, Morris I, Sam C. KRA, Hedgehog, Wnt and the twisted developmental biology of pancreatic ductal adenocaarcinoma. Nat Rev Cancer 2010;10:683-695.

50. Walter D, Venancio O, Buza E. Systematic in vivo inactivation of chromatin-regulating enzymes identifies Setd2 as a potent tumor suppressor in lung adenocarcinoma. Cancer Res 2017;77:1719-1729.

51. Izeradjene K, Combs C, Best M, et al. Kras(G12D) and Smad4/Dpc4 haploinsufficiency cooperate to induce mucinous cystic neoplasms and invasive adenocarcinoma of the pancreas. Cancer Cell 2007;11:229-43.

52. Kopp JL, Dubois CL, Schaeffer DF. Loss of PTEN and Activation of Kras Synergistically Induce Formation of Intraductal Papillary Mucinous Neoplasia From Pancreatic Ductal Cells in Mice. Gastroenterology 2018; doi: 10.1053/j.gastro.2017.12.007.

Author names in bold designate shared co-first authorship.

Figure legends

Figure 1. *Arid1a* loss in the murine pancreata results in the formation of cysts.

(A–C) From the top, a macroscopic image, hematoxylin and eosin (H&E) and ARID1A staining. (D, pancreatic duct; broken line, islet; D1, ARID1A-positive duct; D2, ARID1A-negative duct; C, pancreatic cyst) (A) Wild-type (n = 8) (B) *Ptf1a-Cre; Arid1a*$^{f/+}$ pancreata (n = 10) showed no abnormalities. (C) *Ptf1a-Cre; Arid1a*$^{f/f}$ pancreata (n = 21) developed cystic formations. (D) Molecular characterization of the cystic lesions in the *Ptf1a-Cre; Arid1a*$^{f/f}$ pancreata. All white scale bars = 1 cm. All black scale bars = 50 μm.

Figure 2. *Arid1a* deletion collaborates with mutant *Kras* to form neoplastic cystic lesions that resemble human IPMN.

(A) Macroscopic image of control *Ptf1a-Cre; Kras*^{G12D}*; Arid1a*$^{f/+}$ (duodenum + pancreas + spleen) (n = 10) and *Ptf1a-Cre; Kras*^{G12D}*; Arid1a*$^{f/f}$ mice (pancreas + spleen) (n = 43).

(B) Relative pancreatic weight (PW) to body weight (BW) ratio of *Ptf1a-Cre; Kras^{G12D}; Arid1a$^{f/+}$* (n = 6) and *Ptf1a-Cre; Kras^{G12D}; Arid1a$^{f/f}$* (n = 6) mice.

(C) From the top, hematoxylin & eosin, cytokeratin, amylase, and alcian blue staining of *Ptf1a-Cre; Kras^{G12D}; Arid1a$^{f/+}$* and *Ptf1a-Cre; Kras^{G12D}; Arid1a$^{f/f}$* mice. The arrowhead denotes a connection between the cystic lesion and pancreatic ductal system. (D) From the top, ARID1A, phospho-p44/42 MAPK (Thr202/Tyr204) (pERK1/2), Ki67 staining of control *Ptf1a-Cre; Kras^{G12D}; Arid1a$^{f/+}$* and *Ptf1a-Cre; Kras^{G12D}; Arid1a$^{f/f}$* mice.

(E) Mucin expression pattern of IPMN in *Ptf1a-Cre; Kras^{G12D}; Arid1a$^{f/f}$* mice. White scale bars = 1 cm. Black scale bars = 50 μm.

Figure 3. IPMN in *Ptf1a-Cre; Kras^{G12D}; Arid1a$^{f/f}$* mice exhibit varying grades of dysplasia and progress to PDAC

(A) IPMN with low- and high-grade dysplasia in *Ptf1a-Cre; Kras^{G12D}; Arid1a$^{f/f}$* mice at 18 weeks of age. (B) Incidence of PDAC formation in *Ptf1a-Cre; Kras^{G12D}; Arid1a$^{f/f}$* (n = 43), *Ptf1a-Cre; Kras^{G12D}* (n = 8), and *Ptf1a-Cre; Kras^{G12D};*

739 *Arid1a*$^{f/f}$ (n = 16) mice at indicated time points. (C) Two images on the left show
740 IPMN with severe-grade dysplasia at 48 weeks of age. Two images on the right
741 show invasive adenocarcinoma developed from IPMN in *Ptf1a-Cre; Kras*^{G12D}*;*
742 *Arid1a*$^{f/f}$ mice at 48 weeks of age. (D) ARID1A, pERK1/2, Ki67, and PDX1
743 staining in PDAC cells in *Ptf1a-Cre; Kras*^{G12D}*; Arid1a*$^{f/f}$ mice.
744 Scale bars = 50 μm.
745
746 **Figure 4. *Arid1a*-deficient IPMN originates from the pancreatic ductal cells**
747 **but not from acinar cells.**
748 (A) Schema of recombination in *Ptf1a-Cre*^{ERT2}*; Kras*^{G12D}*; Arid1a*$^{f/f}$ mice.
749 (B) Tamoxifen and caerulein administration schema for experiments using
750 *Ptf1a-Cre*^{ERT2}*; Kras*^{G12D}*; Arid1a*$^{f/+}$ (n = 5) and *Ptf1a-Cre*^{ERT2}*; Kras*^{G12D}*; Arid1a*$^{f/f}$
751 mice (n = 5).
752 (C) *Ptf1a-Cre*^{ERT2}*; Kras*^{G12D}*; Arid1a*$^{f/+}$ and *Ptf1a-Cre*^{ERT2}*; Kras*^{G12D}*; Arid1a*$^{f/f}$ mice
753 developed multiple PanIN but not IPMN.
754 (D) Schema of recombination in *Hn1fb-Cre*^{ERT2}*; Kras*^{G12D}*; Arid1a*$^{f/f}$ mice.

(E) Tamoxifen administration schema for experiments using *Hn1b-Cre^{ERT2}; Kras^{G12D}; Arid1a$^{f/+}$* (n = 5) and *Hn1b-Cre^{ERT2}; Kras^{G12D}; Arid1a$^{f/f}$* mice (n = 6).

(F) The upper figures show that *Arid1a* deletion in the presence of mutant *Kras* in PDC resulted in a cystic neoplastic lesion. The lower figures show that the mucin expression patterns of the cystic lesions in *Hnf1b-Cre^{ERT2}; Kras^{G12D}; Arid1a$^{f/f}$* mice were similar to those in *Ptf1a-Cre; Kras^{G12D}; Arid1a$^{f/f}$* mice.

Scale Bar = 50 μm

Figure 5. *Arid1a* deletion leads to reduction in *Sox9* expression, dedifferentiation of PDCs, and duct dilation, and ectopic expression of *Sox9* prevents the dedifferentiation of PDCs and duct dilation *ex vivo*.

(A) SOX9 staining in wild type (WT), *Ptf1a-Cre; Arid1a$^{f/f}$*, *Ptf1a-Cre; Kras^{G12D}; Arid1a$^{f/f}$*, and *Hnf1b-Cre^{ERT2}; Kras^{G12D}; Arid1a$^{f/f}$* mice.

(B) Schemas of adenovirus infection experiments. +Ad-GFP, control GFP expressing adenovirus transmission; +Ad-Cre, Cre recombinase and GFP expressing adenovirus transmission.

(C, D) Images of 3D culture of PDCs isolated from *Arid1a*$^{f/f}$ and *Arid1a*$^{f/f}$*; Sox9OE* mice. Diameters of the cysts formed by PDCs are shown in bar graphs. (E) q-PCR analysis of components of the SWI/SNF (*Arid1a* and *Brg1*) complexes, duct cell markers [mouse *Sox9* (mo*Sox9*), human *Sox9* (hu*SOX9*), *Krt19*, and *Hnf1b*], and progenitor cell markers (*Gata4*, *Gata6*, and *Hes1*) in cultured PDCs isolated from *Arid1a*$^{f/f}$ (n = 3) and *Arid1a*$^{f/f}$*; Sox9OE* mice (n = 3) and infected by adenoviruses.

Scale Bar = 50 μm

$P < 0.05$ and $P < 0.01$ were represented with single and double asterisks, respectively.

Figure 6. The mTOR pathway activity is lower in *Arid1a*-deficient IPMN compared to that in *Brg1*-deficient IPMN.

(A) BRG1 expression in *Ptf1a-Cre; Kras*^{G12D}*; Arid1a*$^{f/f}$ mice (n = 6) and ARID1A expression in *Ptf1a-Cre; Kras*^{G12D}*; Brg1*$^{f/f}$ mice (n = 6).

786 (B) Schema of microarray analysis of IPMN in *Ptf1a-Cre; Kras^{G12D}; Arid1a$^{f/f}$* (n =
787 2) and *Ptf1a-Cre; Kras^{G12D}; Brg1$^{f/f}$* (n = 3) mice. Seven gene sets were
788 significantly upregulated in *Ptf1a-Cre; Kras^{G12D}; Arid1a$^{f/f}$* mice compared to those
789 in *Ptf1a-Cre; Kras^{G12D}; Brg1$^{f/f}$* mice. The AKT_UP_MTOR_DN.V1_UP gene set
790 contains genes upregulated by everolimus in mouse prostate tissue
791 transgenically expressing the human *AKT1* gene versus untreated controls.
792 (C) Phosphorylated S6 (pS6) was barely observed in IPMN in *Ptf1a-Cre;*
793 *Kras^{G12D}; Arid1a$^{f/f}$* mice, whereas it was generally observed in PanIN in
794 *Ptf1a-Cre; Kras^{G12D}* mice, IPMN in *Ptf1a-Cre; Kras^{G12D}; Brg1$^{f/f}$* mice, and PDAC
795 in *Ptf1a-Cre; Kras^{G12D}; Arid1a$^{f/f}$* mice.
796 (D) q-PCR analysis of the components of the mTor pathway in PDCs with *Arid1a*
797 deletion.
798 Scale Bar = 50 μm
799 $P < 0.05$ and $P < 0.01$ were represented with single and double asterisks,
800 respectively. $P > 0.05$ was represented by a number sign.
801

Figure 7. Absence of ARID1A expression is observed in subsets of human IPMN, and ARID1A expression is positively correlated with expression of SOX9 and components of the mTOR pathway in human IPMN and PDAC.

(A) Histological analysis of human IPMN (n = 58) by ARID1A, SOX9, and pS6 staining.

(B) Spearman's rank correlation coefficient between *ARID1A* expression and components of the mTOR pathway in human PDAC.

(C) Plots of mRNA expression of *ARID1A* and components of the mTOR pathway.

Scale Bar = 50 μm.

Figure1

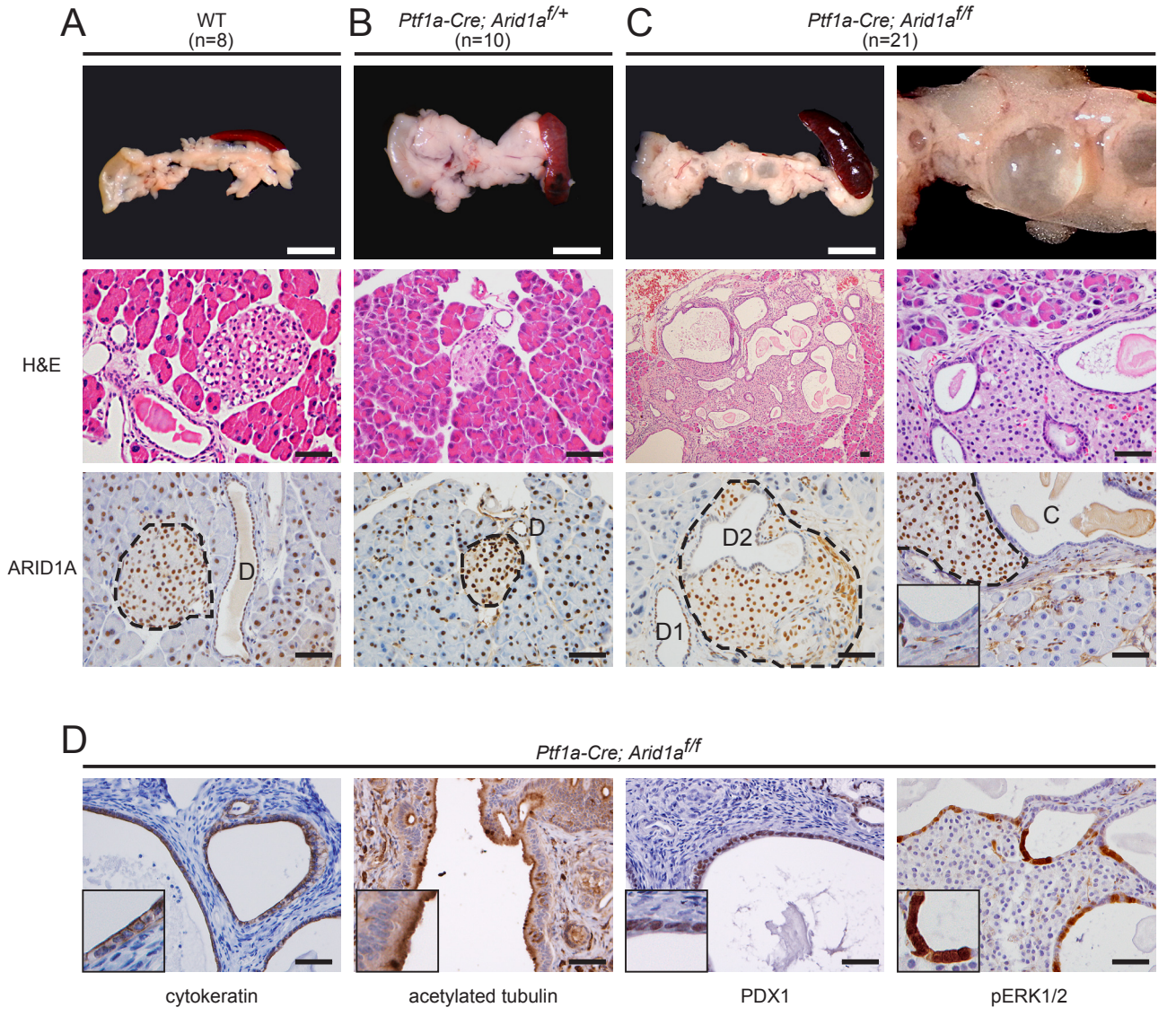
A
WT
(n=8)
B
Ptf1a-Cre; Arid1a f/+
(n=10)
C
Ptf1a-Cre; Arid1a f/f
(n=21)
H&E
ARID1A
D
D
D2
D1
C

D
Ptf1a-Cre; Arid1a f/f
cytokeratin
acetylated tubulin
PDX1
pERK1/2

Figure2

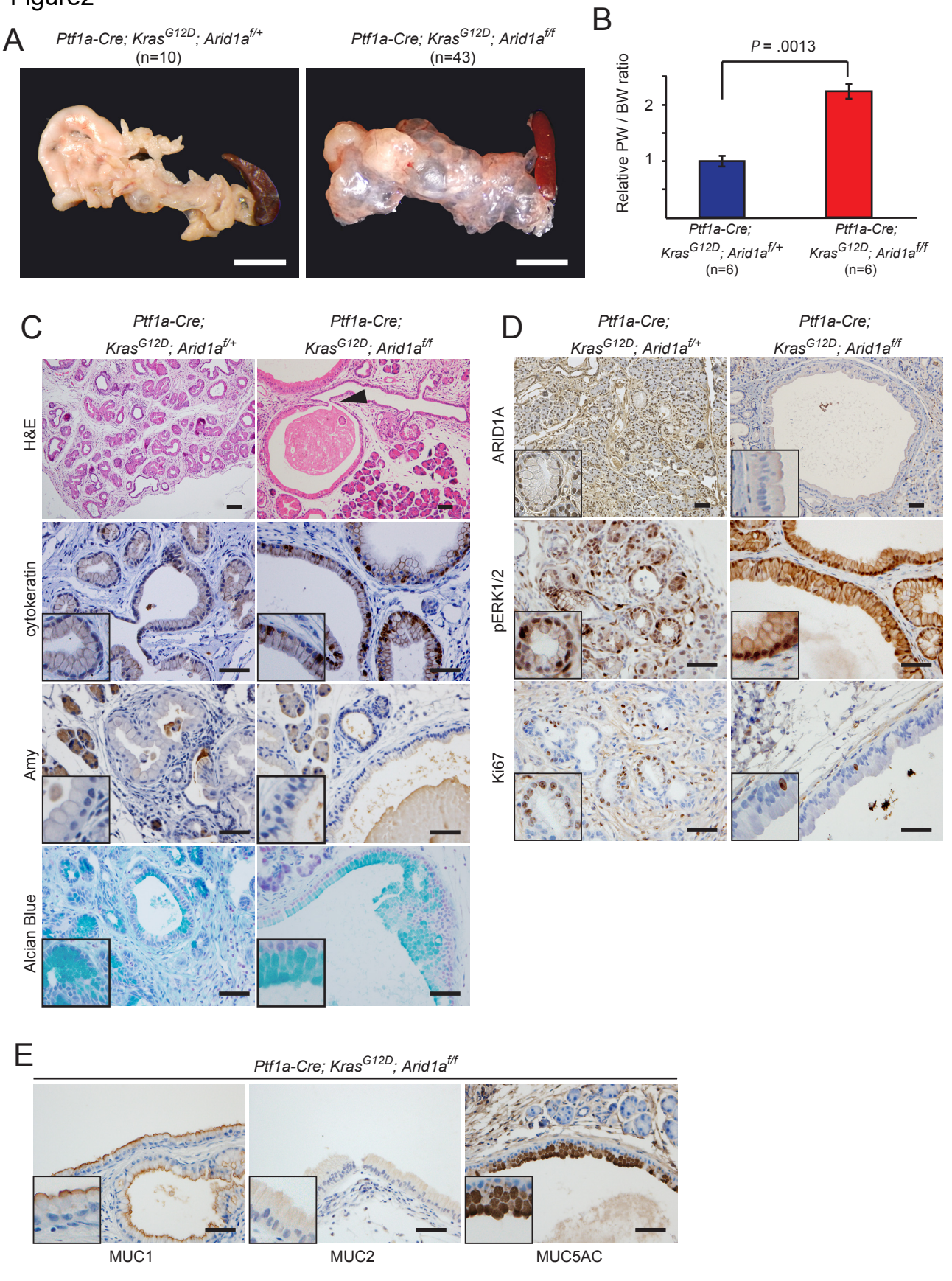
A
Ptf1a-Cre; KrasG12D; Arid1af/+
(n=10)
Ptf1a-Cre; KrasG12D; Arid1af/f
(n=43)
B
P = .0013
Relative PW / BW ratio
2
1
Ptf1a-Cre; KrasG12D; Arid1af/+
(n=6)
Ptf1a-Cre; KrasG12D; Arid1af/f
(n=6)
C
Ptf1a-Cre; KrasG12D; Arid1af/+
Ptf1a-Cre; KrasG12D; Arid1af/f
H&E
cytokeratin
Amy
Alcian Blue
D
Ptf1a-Cre; KrasG12D; Arid1af/+
Ptf1a-Cre; KrasG12D; Arid1af/f
ARID1A
pERK1/2
Ki67
E
Ptf1a-Cre; KrasG12D; Arid1af/f
MUC1
MUC2
MUC5AC

Figure3

A

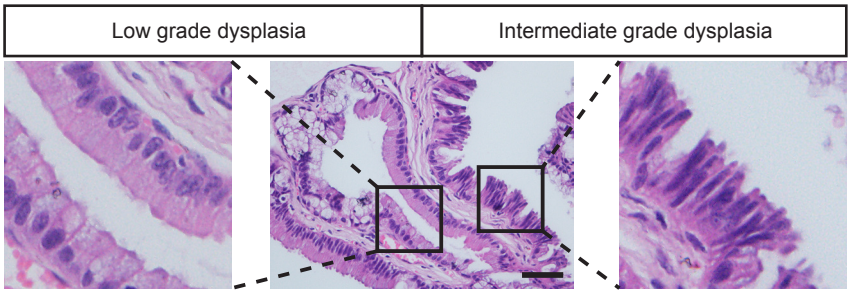

B

Incidence of adenocarcinoma

	Ptf1a-Cre; Kras^{G12D}; Arid1a$^{f/f}$ (n=43)	*Ptf1a-Cre; Kras^{G12D}* (n=8) or *Ptf1a-Cre; Kras^{G12D}; Arid1a$^{f/+}$* (n=16)
14-18 weeks	0% (n=13)	0% (n=8)
20-24 weeks	0% (n=15)	
44-48 weeks	20% (n=15)	0% (n=16)

C

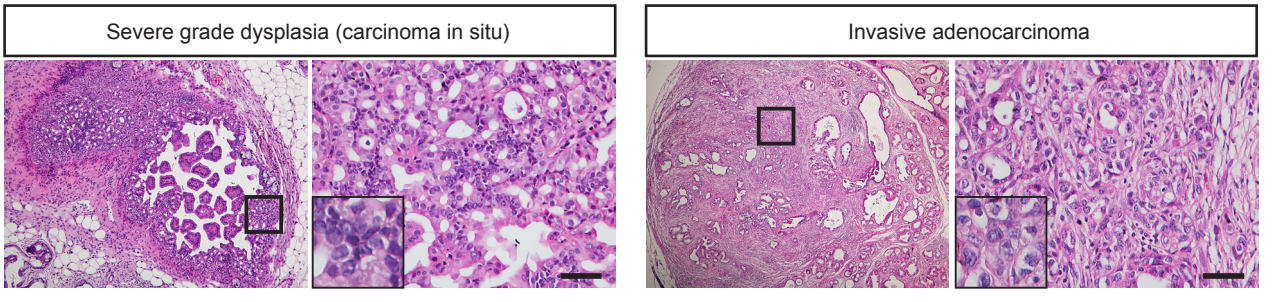

D

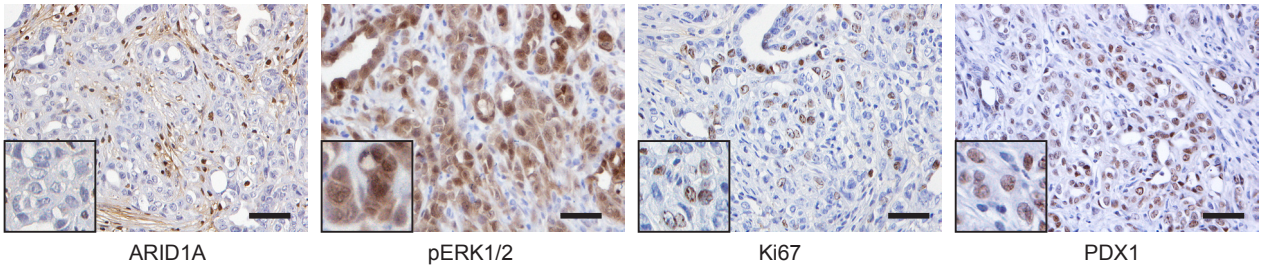

Figure4

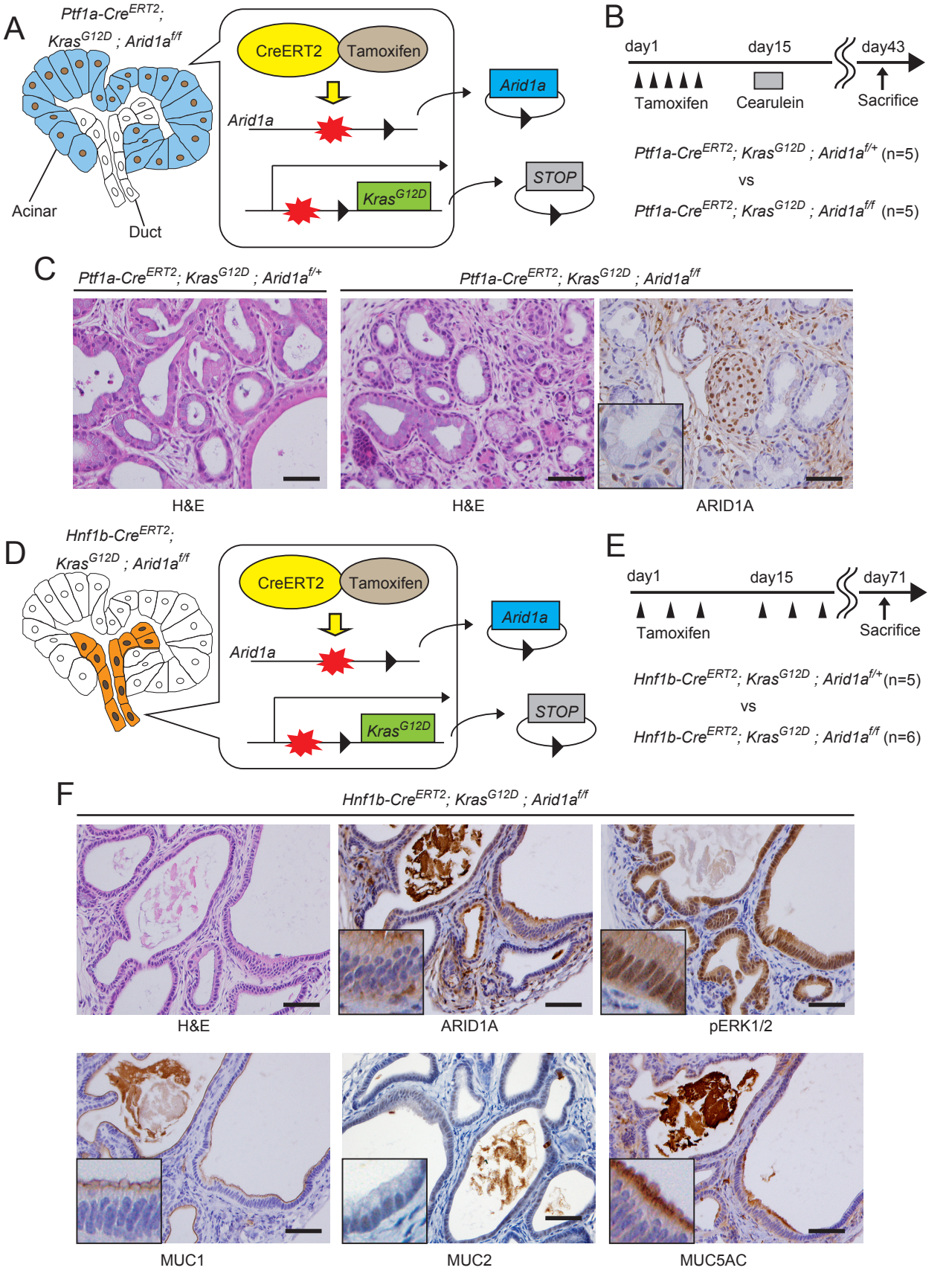
A
Ptf1a-Cre^ERT2;
Kras^G12D ; Arid1a^f/f
Acinar
Duct
CreERT2
Tamoxifen
Arid1a
Arid1a
Kras^G12D
STOP
B
day1
day15
day43
Tamoxifen
Cearulein
Sacrifice
Ptf1a-Cre^ERT2; Kras^G12D ; Arid1a^f/+ (n=5)
vs
Ptf1a-Cre^ERT2; Kras^G12D ; Arid1a^f/f (n=5)
C
Ptf1a-Cre^ERT2; Kras^G12D ; Arid1a^f/+
Ptf1a-Cre^ERT2; Kras^G12D ; Arid1a^f/f
H&E
H&E
ARID1A
D
Hnf1b-Cre^ERT2;
Kras^G12D ; Arid1a^f/f
CreERT2
Tamoxifen
Arid1a
Arid1a
Kras^G12D
STOP
E
day1
day15
day71
Tamoxifen
Sacrifice
Hnf1b-Cre^ERT2; Kras^G12D ; Arid1a^f/+(n=5)
vs
Hnf1b-Cre^ERT2; Kras^G12D ; Arid1a^f/f (n=6)
F
Hnf1b-Cre^ERT2; Kras^G12D ; Arid1a^f/f
H&E
ARID1A
pERK1/2
MUC1
MUC2
MUC5AC

Figure5

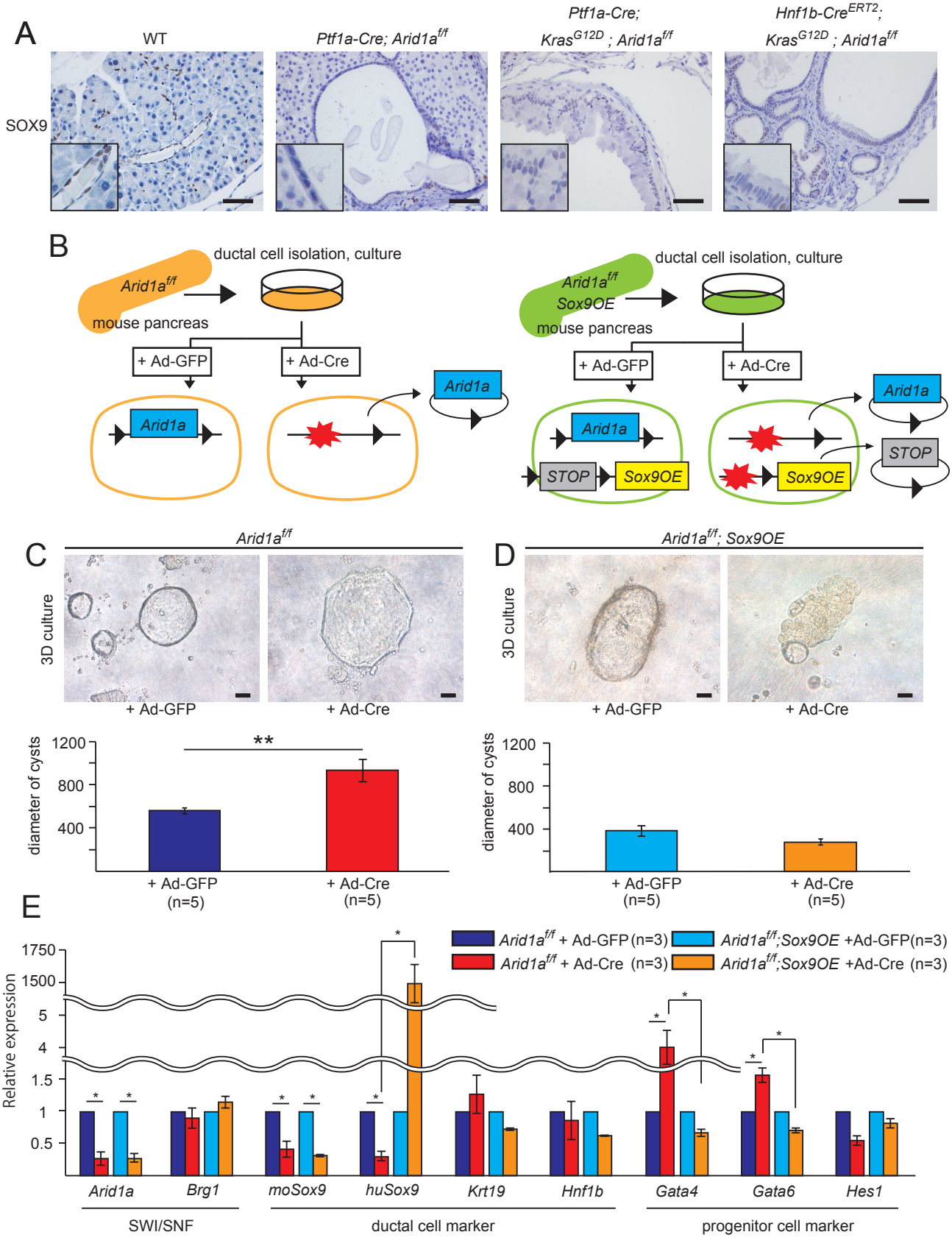
A
WT
Ptf1a-Cre; Arid1a f/f
Ptf1a-Cre; Kras G12D ; Arid1a f/f
Hnf1b-Cre ERT2; Kras G12D ; Arid1a f/f
SOX9
B
ductal cell isolation, culture
Arid1a f/f
mouse pancreas
+ Ad-GFP
+ Ad-Cre
Arid1a
Arid1a f/f Sox9OE
STOP
Sox9OE
C
Arid1a f/f
3D culture
+ Ad-GFP
+ Ad-Cre
diameter of cysts
1200
800
400
**
+ Ad-GFP (n=5)
+ Ad-Cre (n=5)
D
Arid1a f/f; Sox9OE
E
Arid1a f/f + Ad-GFP (n=3)
Arid1a f/f + Ad-Cre (n=3)
Arid1a f/f;Sox9OE +Ad-GFP(n=3)
Arid1a f/f;Sox9OE +Ad-Cre (n=3)
Relative expression
1750
1500
5
4
1.5
1
0.5
Arid1a
Brg1
moSox9
huSox9
Krt19
Hnf1b
Gata4
Gata6
Hes1
SWI/SNF
ductal cell marker
progenitor cell marker

Figure6

A

Ptf1a-Cre; Kras^{G12D}; Arid1a$^{f/f}$ (n=6)

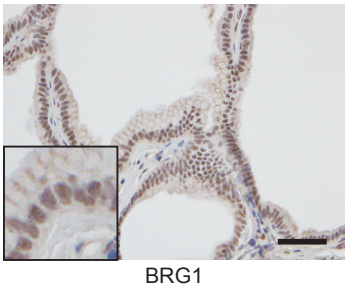

BRG1

Ptf1a-Cre; Kras^{G12D}; Brg1$^{f/f}$ (n=6)

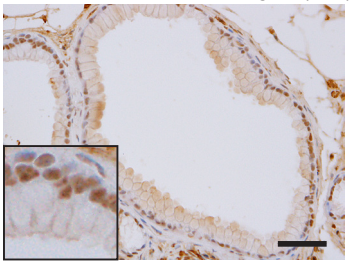

ARID1A

B

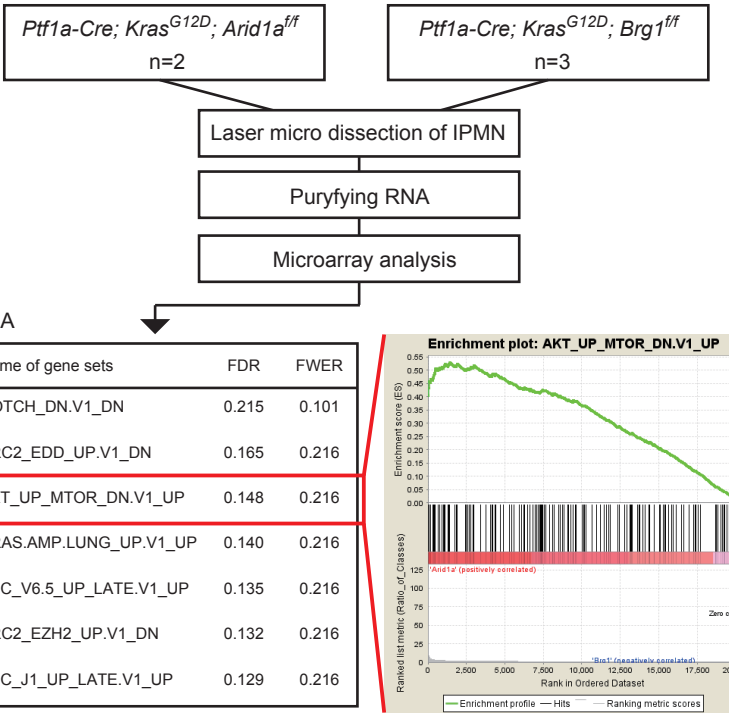

C

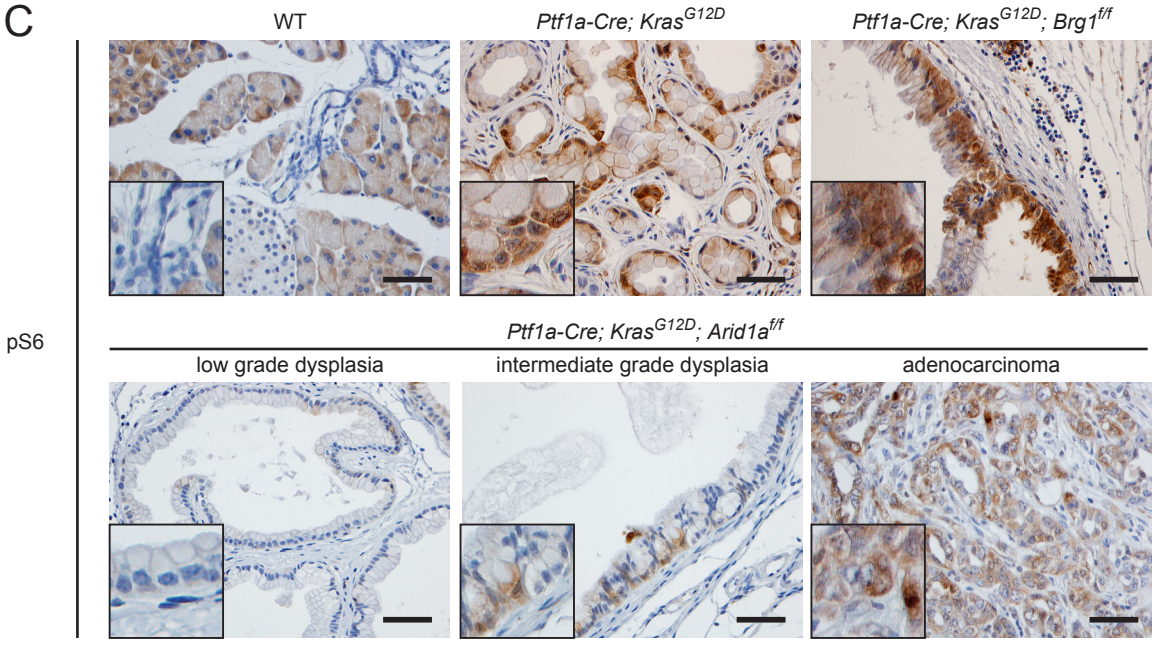

D

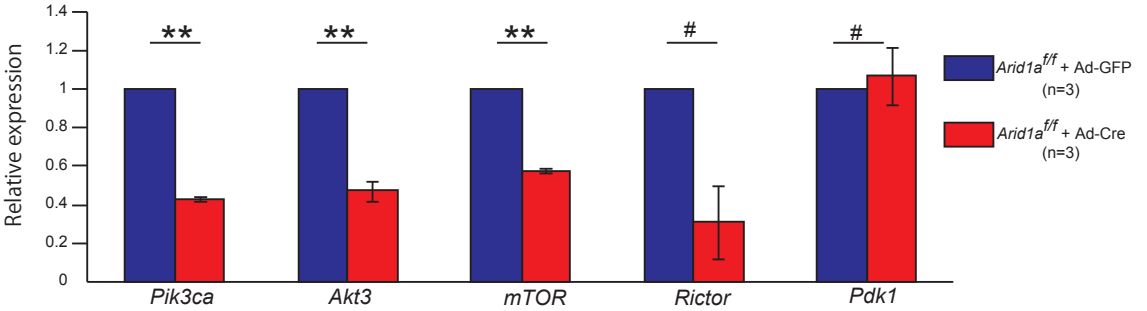

Figure7

A

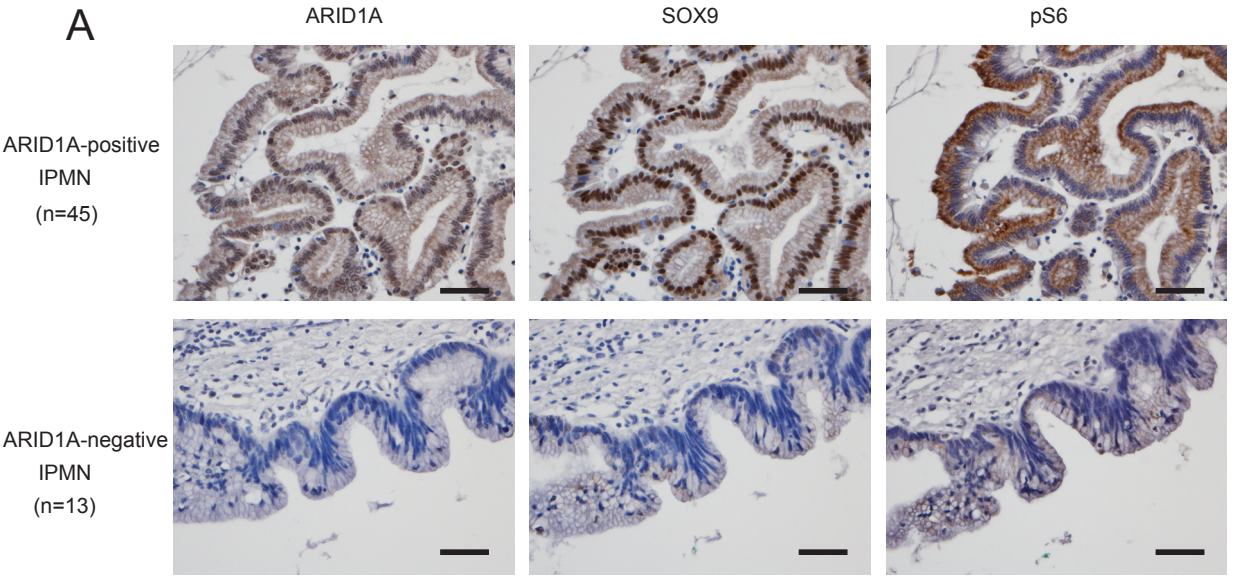

B

gene	spearman
PIK3CA	0.556
PTEN	0.305
PDK1	0.073
PDK2	-0.005
PDK3	0.158
AKT1	-0.113
AKT2	0.028
AKT3	0.463
TSC1	0.298
AKT1S1	-0.409
RHEB	-0.319
RPTOR	0.087
RICTOR	0.501
MTOR	0.63
RPS6KB1	0.225
RPS6	-0.285

C

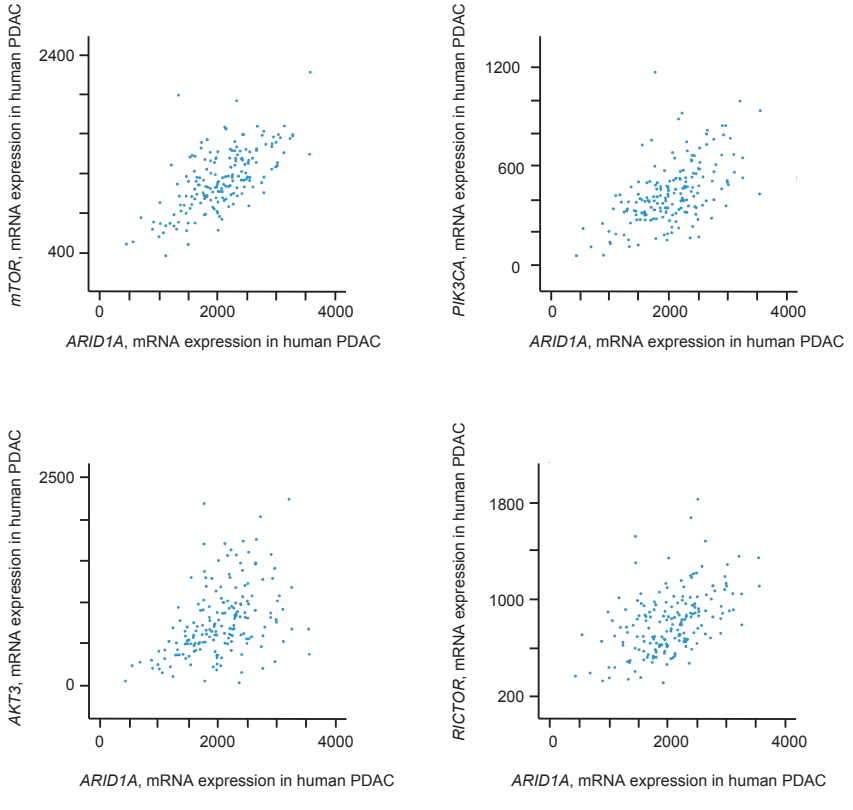

Supplementary Figure1

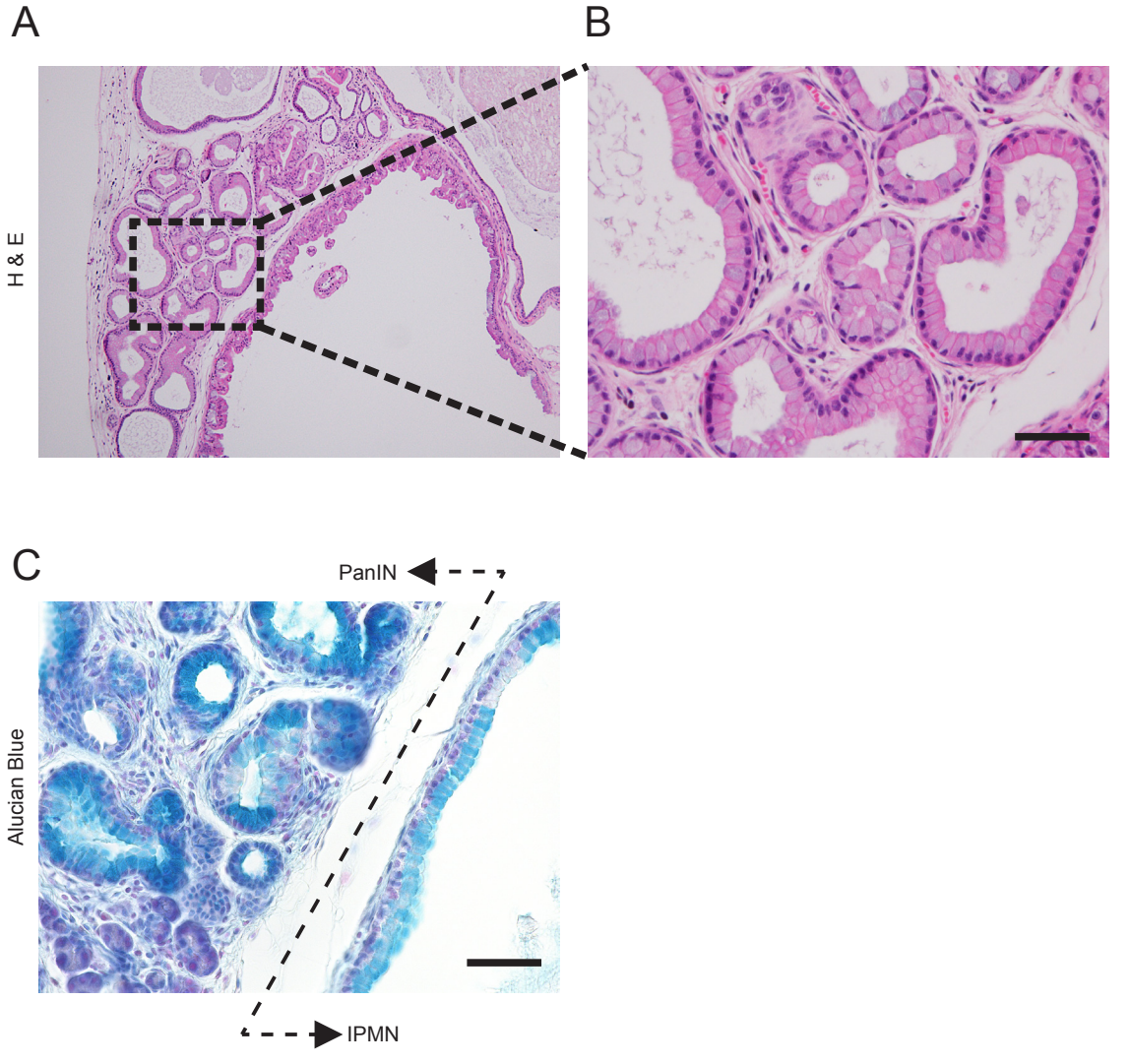

Supplementary Figure2

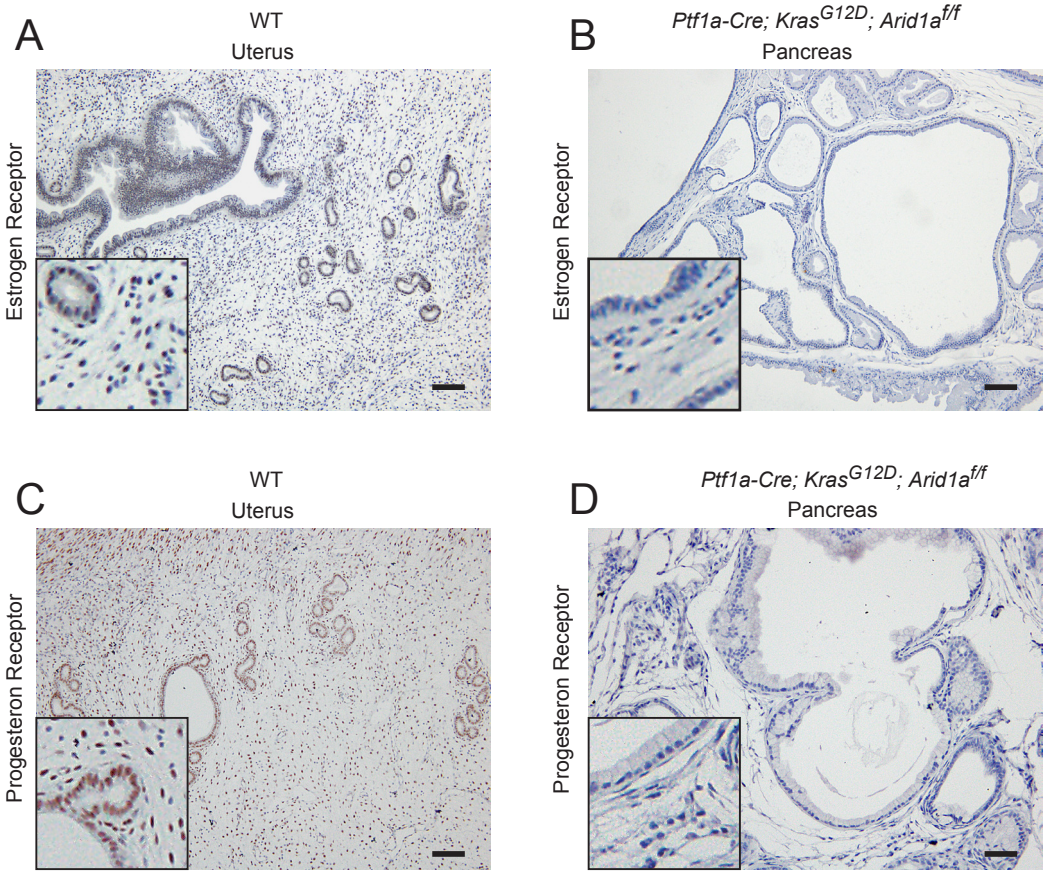

Supplementary Figure3

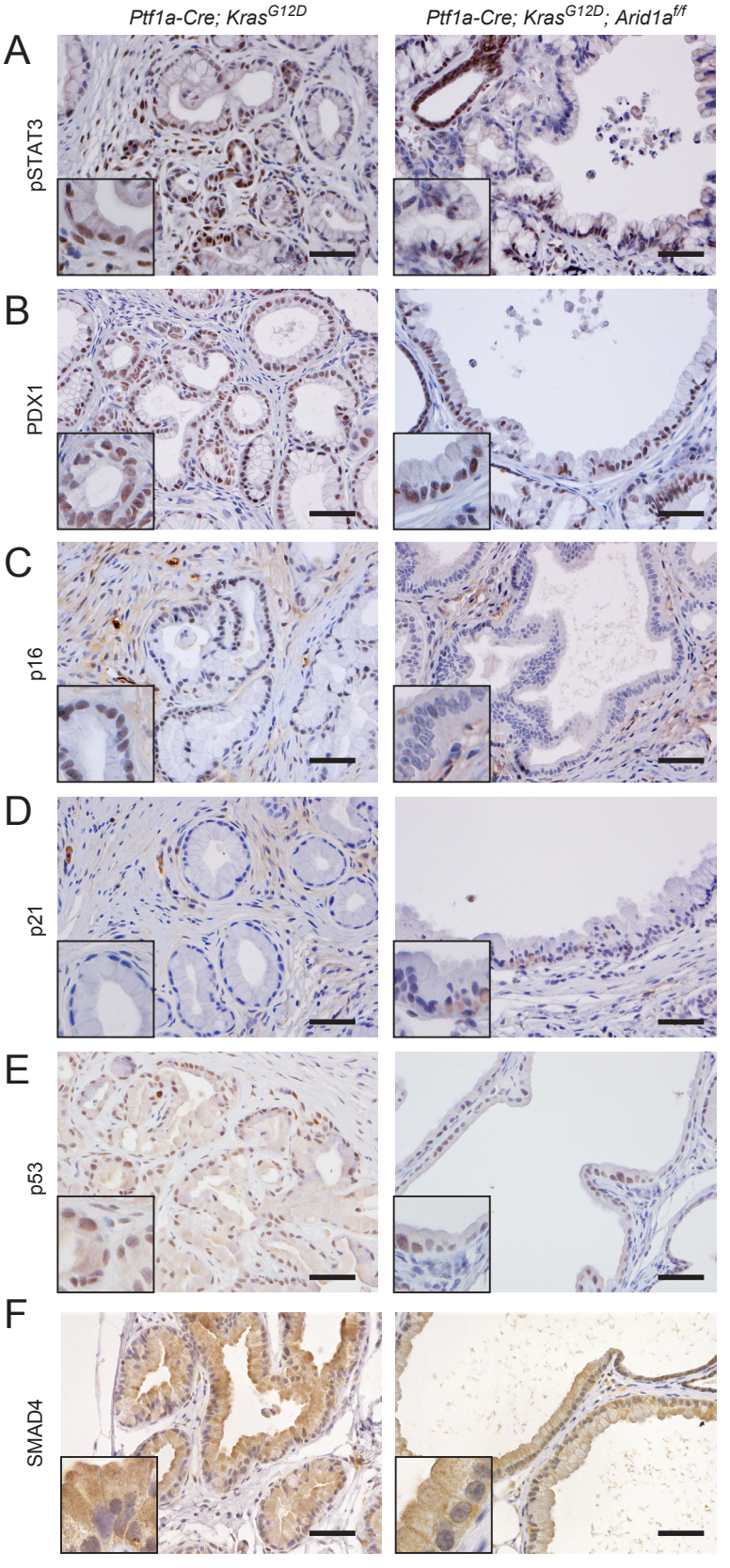

Supplementary Figure4

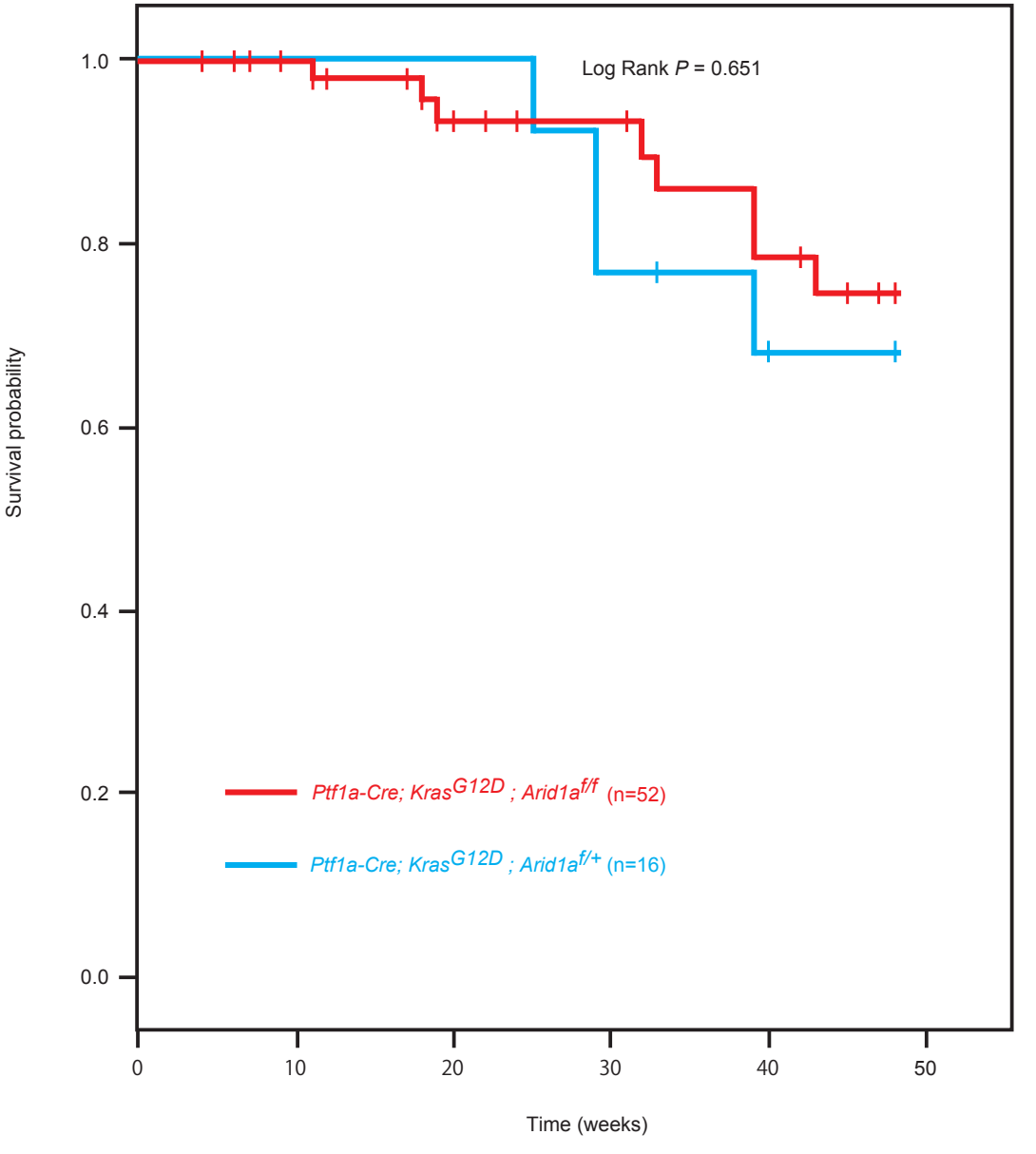

Supplementary Figure5

A

Ptf1a-Cre; Arid1a$^{f/f}$; Sox9OE

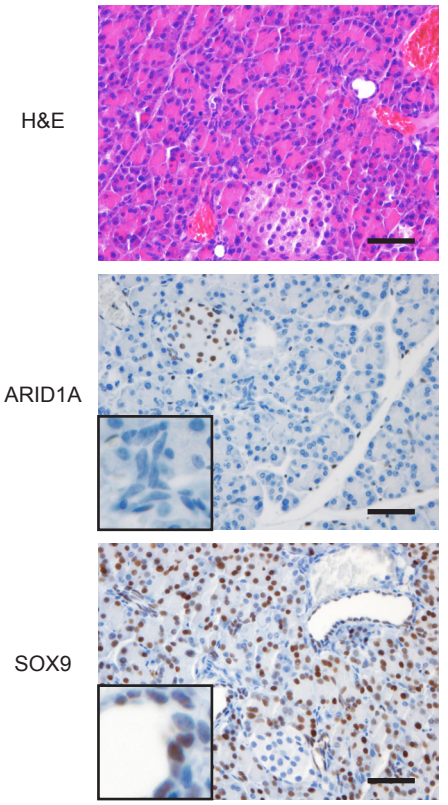

B

Ptf1a-Cre; Kras^{G12D}; Arid1a$^{f/f}$; Sox9OE

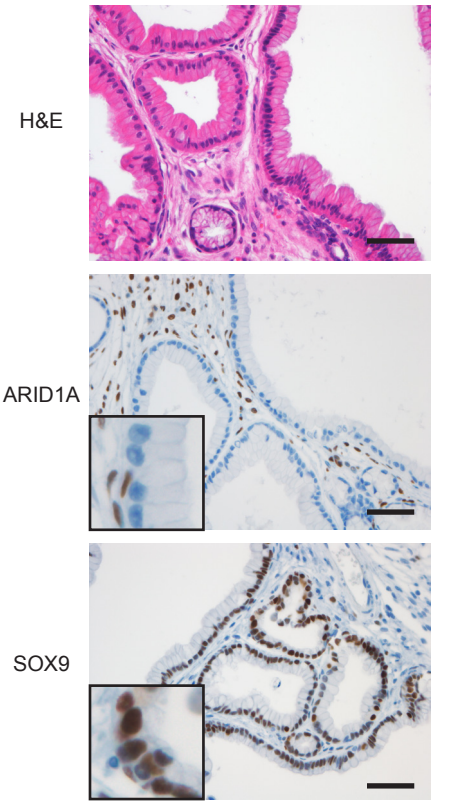

C

	Ptf1a-Cre; Arid1a$^{f/f}$	*Ptf1a-Cre; Arid1a$^{f/f}$; Sox9OE*	*Ptf1a-Cre; Kras^{G12D} ; Arid1a$^{f/f}$*	*Ptf1a-Cre; Kras^{G12D} ; Arid1a$^{f/f}$; Sox9OE*
Dilation of ducts	+	-	+	+
IPMN	-	-	+	+

Supplementary Figure6

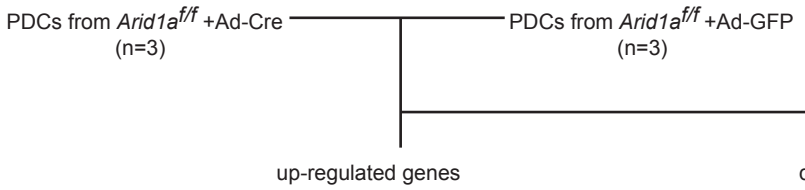

	up-regulated genes	down-regulated genes
pathways with significant difference	Metabolic pathways Neuroactive ligand-receptor interaction Seretonergic synapse MAPK signaling pathway Retional metabolism Ras signalin pathway cAMP signaling pathway Inflammatory mediator regulation of TRP chanels	Pathways in cancer PI3K-Akt signaling pathway Neuroactive ligand-receptor interaction Ras signalin pathway Focal adhesion Endocytosis Cytokine-cytokine receptor interaction Cell adhesion molecules (CAMs)
GO enrichment analysis	Transport Multicellular organism development Oxidation-reduction process Cell differentiation Positive regulation of cell proliferation Ion transport Proteolysis Lipid metabolic processes	Membrane Integral component of membrane Cytoplasm Plasma membrane Extracellular exosome Extracellular region Extracellular space Integral component of plasma membrane

Supplementary Figure7

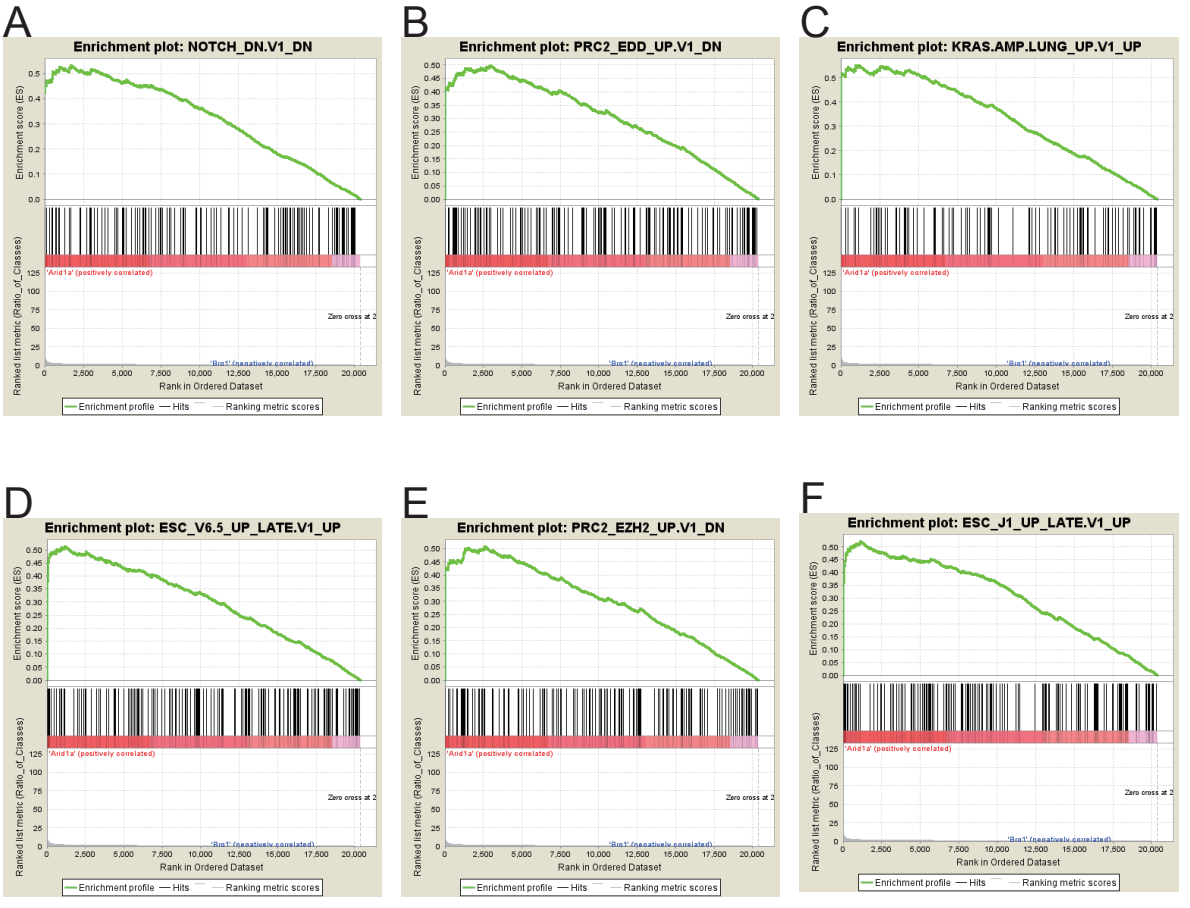

Supplementary Table 1. Summary of clinical and histological characteristics of human IPMN and PDAC

	IPMN			PDAC		
	ARID1A negative	ARID1A positive	*p*	ARID1A negative	ARID1A positive	*p*
number of case	13	45		16	28	
age (mean)	65.6	67.2		69.1	68.9	
sex (male/female)	3.33	1.14		3	1.8	
historogical subtype						
gastric	2 (15.4%)	22 (48.9%)	*			
intestinal	7 (53.8%)	12 (26.7%)				
pancreatobiliary	1 (7.7%)	9 (20.0%)				
oncocytic	3 (23.1%)	0 (0%)	**			
clinical subtype						
branch-duct	3 (23.1%)	11 (24.4%)				
main-duct	6 (46.2%)	16 (35.6%)				
mixed	4 (30.8%)	18 (40.0%)				
adenocarcinoma	10 (76.9%)	23 (51.1%)				
immunohistochemical analysis						
SOX9 positive	5 (38.5%)	38 (84.4%)	**	9 (56.3%)	27 (96.4%)	**
pS6 positive	4 (30.8%)	30 (66.7%)	*	6 (37.5%)	17 (60.7%)	

* $p < 0.05$ ** $p < 0.01$

Supplementary Table 2. Conditions and primary antibodies for immunohistochemistry

Antibody	Supplier	Catalog number	IHC dilation
acetylated tubulin	Sigma	T7451	1:200
Amylase	Abcam	ab21156	1:1000
ARID1A	Abnova	H0000829-M02	1:200
BRG1	Santa cruz	sc-10768	1:1000
wide spectrum cytokeratin	Abcam	ab9377	1:200
Estrogen receptor α	Millipore	06-935	1:400
Ki67	Dako	M7249	1:25
MUC1	Abcam	ab15481	1:200
MUC2	Santa cruz	sc-15334	1:100
MUC5ac	Abcam	ab3649	1:100
pERK 1/2 (phospho-p44/42)	Cell Signaling	4370	1:200
PDX1	Abcam	ab47308	1:1000
progesterone receptor	Thermo	RM-9102-S0	1:1000
pSTAT3	Cell Signaling	9145	1:200
pS6 (Ser235/236)	Cell Signaling	2211	1:400
p16	Santa cruz	sc-1661	1:500
p21	Abcam	ab109199	1:250
p53	Vector Lab	VP-P956	1:500
SOX9	Millipore	AB5535	1:10000

Supplementary Table 3. Sequences of primer sets for quantitative RT-PCR

primer set	Forward	Reverse
Gapdh	AGGTCGGTGTGAACGGATTTG	TGTAGACCATGTAGTTGAGGTCA
Arid1a	GACCCCTCAGTCATCCAGTC	GAGTATGGGTTAGTCCCACCA
Brg1	CAAAGACAAGCATATCCTAGCCA	CACGTAGTGTGTGTTAAGGACC
mo-Sox9	AGTACCCGCATCTGCACAAC	ACGAAGGGTCTCTTCTCGCT
hu-Sox9	AGCGAACGCACATCAAGAC	CTGTAGGCGATCTGTTGGGG
Krt19	GGGGGTTCAGTACGCATTGG	GAGGACGAGGTCACGAAGC
Hnf1b	GTTACTGCCGTCCCCGAATTT	CGGCTTGGTGTCGAGATCC
Gata4	CCCTACCCAGCCTACATGG	ACATATCGAGATTGGGGTGTCT
Gata6	TTGCTCCGGTAACAGCAGTG	GTGGTCGCTTGTGTAGAAGGA
Hes1	ATAGCTCCCGGCATTCCAAG	GCGCGGTATTTCCCCAACA
Pik3ca	CCACGACCATCTTCGGGTG	ACGGAGGCATTCTAAAGTCACTA
Akt3	TGGGTTCAGAAGAGGGGAGAA	AGGGGATAAGGTAAGTCCACATC
mTor	CAGTTCGCCAGTGGACTGAAG	AGACTCCTCCTGACTCATCTCT
Rictor	GCTGCGCTATCTCATCCAAGA	GGGTTCTGAAGTGCTAGTTCAC
Pdk1	GGACTTCGGGTCAGTGAATGC	TCCTGAGAAGATTGTCGGGGA

Supplementary Materials and Methods

Histological analysis

Mouse tissues were fixed with 4% buffered paraformaldehyde solution, embedded in paraffin, and cut into 5-μm sections. Sections were deparaffinized, rehydrated, and stained with hematoxylin and eosin (H&E) or alcian blue and counterstained with Nuclear Fast Red (Kirkegaard & Perry Laboratories). For immunohistochemistry, antigen retrieval was performed by boiling the sections in primarily 10 mM citric acid buffer with pH 6.0 for 15 min. The sections were washed with phosphate-buffered saline. Blocking was performed using Protein Block Serum-Free (Dako, catalog no. X0909). For primary antibodies, incubation was performed overnight at 4 °C in a humidified chamber; secondary antibody incubation was performed for 1 h at room temperature. Immunoperoxidase labeling was performed with the Vectastain ABC kit (Vector Laboratories, catalog no. PK-6102), and the sections were then subjected to chromophore treatment with diaminobenzidine (DAB) substrate (Dako, catalog no. K3468) and were counterstained with hematoxylin. Primary antibodies are listed in Supplementary Table 2.

Tamoxifen and caerulein treatment

Tamoxifen (Sigma-Aldrich, St Louis, MO, USA) was administered by subcutaneous injection to *Ptf1a-Cre^{ERT2}* mice at a dose of 4 mg/body weight per injection and by oral gavage to *Hnf1b-Cre^{ERT2}* mice at a dose of 10 mg/body weight per gavage. Time courses and the amount of injections/gavages are outlined in Figure 4. Acute pancreatitis was induced by intraperitoneal injection of 50 μg/kg caerulein (diluted in saline; Sigma-Aldrich) on two consecutive days once every hour for 8 h each day.

Adenoviral infection

The single-cell suspension of PDCs was prepared by digesting the 2D-cultured PDCs and the collagen layer with collagenase type V followed by trypsinization. For adenoviral infection, PDCs were incubated at 37 °C with green fluorescent protein (GFP)-expressing adenovirus (Ad-GFP) or Cre recombinase and GFP-expressing adenovirus (Ad-Cre) at a multiplicity of infection of 50 on the collagen-

coated plates overnight. The PDC full medium was replaced every two days.

RNA isolation from cultured cells and quantitative RT-PCR (qPCR)

RNA was isolated using the RNeasy Mini kit (Qiagen, Valencia, CA, USA). Single-stranded cDNA was prepared using the ReverTra Ace qPCR RT kit (Toyobo, Osaka, Japan). qPCR was performed with a SYBR Green-based gene expression assay using the LightCycler 480 system (Roche, Madison, WI, USA). Expression levels were normalized to *GAPDH* levels using the ΔCt method. Primer sequences are described in Supplementary Table 3. All reactions were performed in triplicates.

Laser capture micro-dissection and RNA extraction

The resected pancreas was immersed in the RNAlater solution (Ambion) overnight at 4 °C and then embedded in Frozen Section Compound (Leica) and stored at −80 °C. Frozen specimens were cut into 10-μm sections using a CM1950 cryostat (Leica) and embedded on frame slides (Leica). The sections

were fixed in a 19:1 ethanol and acetic acid mixture, incubated for 3 min on an ice bath, and then washed in ultra-pure distilled water (Invitrogen) for 1 min. For each mouse, 5–6 lesions were selected, and their RNA was extracted using the RNeasy Micro kit (Qiagen, Valencia, CA, USA). After drying, the sections were dissected using the LMD-3500 (Leica) laser-capture micro-dissection system, as previously described[1]. Total RNA was extracted from the dissected tissue using the RNeasy Micro Kit (Qiagen).

Microarray analysis

The quality of RNA extracted from adenovirus-infected PDCs and epithelial cells of IPMNs was examined with an Agilent 2100 bioanalyzer (Agilent Technologies). The epithelial cells of IPMNs were obtained using a laser-capture micro-dissection system (Leica). The RNA integrity numbers of the RNA samples used in the microarray analysis were above 7. The RNA samples were labeled with SureTag Complete DNA Labeling Kit (Agilent Technologies) and hybridized to the SurePrint G3 Mouse GE 8x60K Microarray Kit (Agilent Technologies) using the

Gene Expression Hybridization Kit (Agilent Technologies). The raw data were quantified by Agilent Feature Extraction software (Agilent Technologies). Quantified data were normalized by Gene Spring 12.5 software (Agilent Technologies). Unnamed genes were excluded. As previously described, gene expression data of the epithelial cells of IPMNs were analyzed using Gene Set Enrichment Analysis (GSEA) software and the Molecular Signature Database (MSigDB), which is provided by the Broad Institute of MIT and Harvard[2, 3]. The pathway analyses and Gene Ontology (GO) enrichment analyses of the gene expression data of adenovirus-infected PDCs were performed using DAVID 6.8.[4, 5]

Statistical analysis

Data are presented as means ± SEM. To determine P-values for the qPCR analysis of ductal cell culture experiments, Welch's t-test was performed. To determine P-values for other experiments, Student's t-test was performed. A P-value <0.05 was considered as statistically significant. All statistical analyses

were performed with either Graph-Pad Prism software (version 6.0, GraphPad, San Diego, CA, USA) or Microsoft Excel.

Supplementary References

1. Emmert-Buck MR, Bonner RF, Smith PD, et al. Laser capture microdissection. Science 1996;274:998-1001.

2. Subramanian A, Tamayo P, Mootha VK, et al. Gene set enrichment analysis: a knowledge-based approach for interpreting genome-wide expression profiles. Proc Natl Acad Sci U S A 2005;102:15545-50.

3. Mootha VK, Lindgren CM, Eriksson KF, et al. PGC-1alpha-responsive genes involved in oxidative phosphorylation are coordinately downregulated in human diabetes. Nat Genet 2003;34:267-73.

4. Huang D, Sherman B, Lempicki R. Systemic and integrative analysis of large gene lists using DAVID Bioinformatics Resources. Nature Protoc 2009;4:44-57.

5. Huang D, Sherman B, Lempicki R. Bioinformatics enrichment tools: paths toward the comprehensive functional analysis of large gene lists. Nuclei Acids Res 2009;37:1-13.

Supplementary Figure 1.

***Arid1a* deletion does not suppress PanIN formation**.

(A) PanIN lesions were frequently observed between IPMN in *Ptf1a-Cre; Kras^{G12D}; Arid1a$^{f/f}$* mice.

(B) Magnified image of (A).

(C) Alcian blue staining

Scale Bar = 50 μm

Supplementary Figure 2.

Cystic lesions in *Ptf1a-Cre; Kras^{G12D}; Arid1a$^{f/f}$* mice do not resemble those of human MCN.

(A) Estrogen receptor staining in the uterus isolated from wild type (WT) mice.

(B) Estrogen receptor staining in the pancreas isolated from *Ptf1a-Cre; Kras^{G12D}; Arid1a$^{f/f}$* mice.

(C) Progesterone receptor staining in the uterus isolated from WT mice.

(B) Progesterone receptor staining in the pancreas isolated from *Ptf1a-Cre; Kras^{G12D}; Arid1a$^{f/f}$* mice.

Scale Bar = 50 μm

Supplementary Figure 3.

Histological analysis of IPMN in *Ptf1a-Cre; Kras^{G12D}; Arid1a$^{f/f}$* mice and PanIN in *Ptf1a-Cre; Kras^{G12D}* mice.

(A) Phospho-Stat3, (B) Pdx1, (C) p16, (D) p21, (E) p53, and (F) Smad4 staining.

Scale Bar = 50 μm

Supplementary Figure 4.

Overall survival analysis of *Ptf1a-Cre; KrasG12D; Arid1af/f* and *Ptf1a-Cre; KrasG12D; Arid1af/+* mice

Overall survival analysis of the indicated mouse genotypes. Kaplan-Meir survival curves and the log-rank test showed no significant difference in the survival rates

between *Ptf1a-Cre; Kras^{G12D}; Arid1a$^{f/f}$* mice (red, n = 52) and *Ptf1a-Cre; Kras^{G12D}; Arid1a$^{f/+}$* mice (blue, n = 16).

Supplementary Figure 5.

Sox9 overexpression offsets the effect of *Arid1a* deletion on pancreatic ductal dilation *in vivo.*

(A) Histological analysis of *Ptf1a-Cre; Arid1a$^{f/f}$; Sox9OE* mice at the age of 9-20 weeks (n = 3). H&E staining and immunohistochemistry for Arid1a and Sox9.

(B) Histological analysis of *Ptf1a-Cre; Kras^{G12D}; Arid1a$^{f/f}$; Sox9OE* mice at the age of 4-8 weeks (n = 4). H&E staining and immunohistochemistry for Arid1a and Sox9.

(C) Summary of the phenotypes in terms of pancreatic ductal dilation and IPMN development of *Ptf1a-Cre; Arid1a$^{f/f}$, Ptf1a-Cre; Arid1a$^{f/f}$; Sox9OE, Ptf1a-Cre; Kras^{G12D}; Arid1a$^{f/f}$* and *Ptf1a-Cre; Kras^{G12D}; Arid1a$^{f/f}$; Sox9OE* mice.

Scale Bar = 50 μm

Supplementary Figure 6.

Schema of the microarray analysis of *Arid1a*-deficient and wild type (WT) pancreatic ductal cells.

Pathway analysis and GO enrichment analysis using DAVID 6.8 revealed up/down-regulated pathways or functions by knockdown of *Arid1a* in pancreatic ductal cells. The top eight pathways or GO terms that were most affected by knockdown of *Arid1a* are listed in the boxes.

Supplementary Figure 7.

Gene set enrichment analysis revealed sets of genes that were differently expressed in *Arid1a*-deficient IPMN compared with *Brg1*-deficient IPMN.

(A) NOTCH_DN.V1_DN; genes downregulated in MOLT4 cells (T-ALL) by DAPT [PubChem ID: 16219261], an inhibitor of the NOTCH signaling pathway.

(B) PRC2_EDD_UP.V1_DN; genes downregulated in TIG3 cells (fibroblasts) on knockdown of embryonic ectoderm development (EED).

(C) KRAS.AMP.LUNG_UP.V1_UP; genes upregulated in epithelial lung cancer cell lines overexpressing KRAS.

(D) ESC_V6.5_UP_LATE.V1_UP; genes upregulated during the late stages of differentiation of embryoid bodies from V6.5 embryonic stem cells.

(E) PRC2_EZH2_UP.V1_DN; genes downregulated in TIG3 cells (fibroblasts) on knockdown of enhancer of zeste homolog 2 (EZH2).

(F) ESC_J1_UP_LATE.V1_UP; genes upregulated during the late stages of differentiation of embryoid bodies from J1 embryonic stem cells.

Supplementary Table 1

Summary of clinical and histological characteristics of human IPMN and PDAC

Supplementary Table 2

Conditions and primary antibodies for immunohistochemistry

Supplementary Table 3

Sequences of primer sets for quantitative RT-PCR